

Nitrogen dynamics and nitrate stable isotopes indicate nitrogen loss in the Bay of Bengal

Gesa Schulz^{1,2}, Kirstin Dähnke², Tina Sanders², Jan Penopp¹, Hermann W. Bange³, Rena Czeschel⁴ and Birgit Gaye¹

5 ¹Institute of Geology, University of Hamburg, Hamburg, 20146, Germany

²Institute of Carbon Cycles, Helmholtz-Zentrum Hereon, Geesthacht, 21502, Germany

³Marine Biogeochemistry Research Division, GEOMAR Helmholtz Centre for Ocean Research Kiel, Kiel, 24148, Germany

⁴Ocean Circulation and Climate Dynamics Research Division, GEOMAR Helmholtz Centre for Ocean Research Kiel, Kiel, 24148, Germany

10 *Correspondence to:* Gesa Schulz (Gesa.Schulz@uni-hamburg.de)

Abstract. Oxygen minimum zones (OMZ) play an important role for the global oceanic nitrogen cycle because they account for 20 to 40 % of the global loss of bioavailable nitrogen despite covering only about 1 % of the global ocean volume. The intermediate waters of the Bay of Bengal (BoB) host one of the most pronounced OMZs with near-anoxic conditions. However, it has not yet been recognized as a site with significant nitrate reduction. In this study, we examined the nitrogen cycling processes in the East Equatorial Indian Ocean (EEIO) and the BoB by measuring water column properties, including temperature, salinity, oxygen and nutrient concentrations, as well as nitrate isotope signatures, collected during the SO305 BIOCAT-II/OE2 cruise in April and May 2024. Potential temperature and salinity profiles showed distinct water masses and limited mixing between BoB and the EEIO at 5°N.

15 Nitrate stable isotope depth profiles varied significantly, driven by water mass distribution below 300 m and in-situ fractionation above 300 m. Phytoplankton uptake acts as a nitrate sink in the surface waters, showing a significant isotopic enrichment and nitrogen deficit. In subsurface waters, nitrification was observed, primarily through regenerative production using previously assimilated biomass rather than newly fixed nitrogen from N₂ fixation. Within the OMZ of the BoB, we identified a persistent nitrogen deficit and slightly enriched nitrate isotopes between 100 and 300 m, indicating a nitrogen loss, which we attributed to anammox as the dominant nitrogen loss pathway in the BoB.

25 1 Introduction

Nitrogen is an essential nutrient for all organisms. However, in its most abundant form, unreactive dinitrogen gas (N₂), it is unavailable for most organisms. Through N₂ fixation, N₂ is converted to organic nitrogen, making it bioavailable (Gruber, 2008). This bioavailable nitrogen is removed via denitrification and anammox (Fig. 1), creating N₂. The balance between N₂ fixation and nitrogen loss controls the availability of bioavailable nitrogen in the ocean, and consequently marine productivity (Gruber, 2008).

Denitrification is a stepwise dissimilatory process, which can either be heterotrophic or autotrophic, that reduces nitrate (NO_3^-) to N_2 via nitrite (NO_2^-), nitric oxide (NO) and nitrous oxide (N_2O) (Knowles, 1982; Tiedje, 1988). During anammox (anaerobic ammonium oxidation) ammonium and nitrite are combined to produce N_2 (Strous et al., 1999; Trimmer et al., 2003). In addition to these loss processes, bioavailable nitrogen can be recycled. During assimilation, phytoplankton either uses nitrate or ammonium (NH_4^+) to build biomass. This biomass is transformed back to ammonium through remineralisation, which subsequently can be further oxidized to nitrate via nitrification, with nitrite as an intermediate product (Fig. 1; Gruber, 2008).

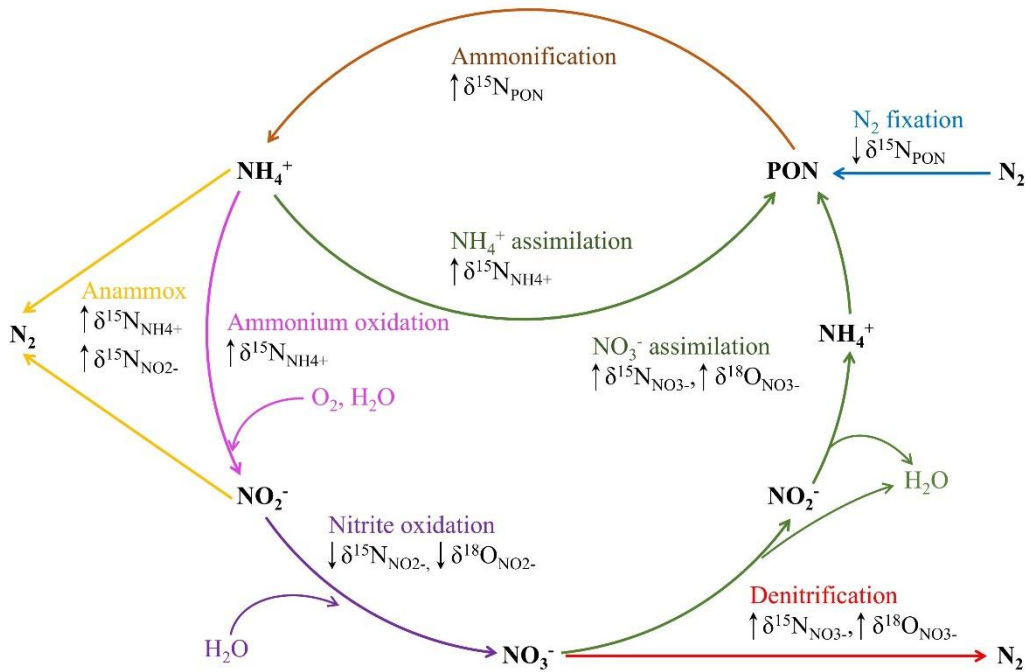


Figure 1: Schematic overview of the nitrogen cycle with isotopic changes caused by N and O fractionation adapted from Casciotti (2016). Abbreviations: Particulate organic nitrogen (PON), ammonium (NH_4^+), nitrite (NO_2^-), nitrate (NO_3^-), dinitrogen (N_2), water (H_2O), and oxygen (O_2).

Nitrogen loss processes are inhibited by the presence of oxygen, which is why oxygen minimum zones (OMZ, with oxygen concentrations $<20 \mu\text{M}$) account for about 30 % of fixed nitrogen loss, despite only covering 1 % of the global ocean (DeVries et al., 2012). Anammox has in some cases been observed to tolerate oxygen concentrations up to $20 \mu\text{M}$ (Kalvelage et al., 2011) and denitrification up to oxygen concentrations of $6 \mu\text{M}$ (Bristow et al., 2016). However, in OMZ waters, the rates of both processes increase only at oxygen concentrations $<1 \mu\text{M}$. However, the oxygen thresholds of denitrification and anammox are still associated with a high degree of uncertainty (Bristow et al., 2016; Dalsgaard et al., 2014; Kalvelage et al., 2011; Rixen et al., 2020). This also applies to nitrification, which usually occurs under oxic conditions, but can also occur in niches with extremely low oxygen concentrations (Sun et al., 2021, 2023). A profound knowledge of the nitrogen turnover processes in

OMZs and their regulation by ambient dissolved oxygen concentrations is essential to understand the global oceanic nitrogen
50 cycle.

The northern East Indian Ocean with its marginal sea, the Bay of Bengal (BoB), hosts one of the most pronounced OMZs in
intermediate waters worldwide, with oxygen concentrations close to anoxic conditions (Rixen et al., 2020; Sridevi and Sarma,
2020). Following its discovery (Wyrski, 1971), the BoB's OMZ is well described in literature (Deuser, 1975; Naqvi et al.,
1978; Sen Gupta et al., 1977). Up to date, no study measured signs for significant nitrogen loss in this area (Howell et al.,
55 1997; Rao et al., 1994; Sardessai et al., 2007; Sarma et al., 2013), although, in 2017, Bristow et al. estimated a small nitrogen
loss of $\sim 1.7 \text{ Tg yr}^{-1}$. They hypothesized that more intense nitrogen loss was likely inhibited by variable oxygen concentrations
within the BoB (Bristow et al., 2017; Johnson et al., 2019). Currently, it is discussed whether the BoB is on the verge of
becoming functional anoxic and may thus evolve towards a significant oceanic nitrogen sink in the future (Bristow et al., 2017;
Rixen et al., 2020; Sarma and Udaya Bhaskar, 2018; Sridevi and Sarma, 2020).

60 Natural variations in nitrate dual isotopes (nitrogen and oxygen) are a commonly used tool to study the marine nitrogen cycle.
Nitrogen turnover processes usually preferably use lighter isotopes, leading to an enrichment of the remaining substrate pool
(Fig. 1). The magnitude of the enrichment is called isotope effect and is process specific. For the isotope effect, we follow the
updated notation of Casciotti et al. (2003). The dual isotope approach uses both nitrogen and oxygen isotopes and allows to
distinguish processes that overlap in $\delta^{15}\text{N}$ alone, so that the nitrogen cycle can be disentangled (Casciotti, 2016; Sigman &
65 Fripiat, 2019). In our study region, nitrate stable isotope measurements are still rare. Relatively recently, Bristow et al. (2017)
analyzed samples in the central and northern BoB, and Harms et al. (2019) and Marshall et al. (2023) presented nitrate stable
isotope data for the subtropical southern Indian Ocean. The East Equatorial Indian Ocean (EEIO) remains largely understudied
compared to other major ocean bodies (Ummenhofer and Hood, 2024). Including the EEIO and BoB in our study allows us to
compare nitrogen turnover across contrasting oxygen regimes and to assess regional differences in nitrate transformation
70 pathways.

In this study, we use water column properties (temperature, salinity, oxygen, nutrients and dual stable isotope signatures of
nitrate) to study the nitrogen cycle in both EEIO and the BoB. The major objectives of our study were to 1) determine the
isotopic signatures of dissolved nitrate in the water column, 2) decipher the major factors affecting the isotopic signatures of
dissolved nitrate and 3) identify the major nitrogen turnover processes (i.e. nitrate production and consumption) in the EEIO
75 and BoB.

2 Methods

2.1 Study site

The Indian Ocean is unique because the Asian landmass forms a northern boundary in the subtropics, which affects the BoB
in many ways. The Asian landmass leads to seasonally reversing monsoon winds in the northern Indian Ocean, which reverse
80 direction from south-westerly winds in summer (June to August) to north-easterly winds in winter (December to February).

The upper surface circulation in the BoB and the zonal current system along the equator are strongly affected by the reversing monsoon system.

85 In the EEIO (located between 05°S-05°N and 80°E-100°E; Fig. 2), westerly winds emerge during the transition phase in spring (April and May), and again in fall (October and November) leading to strong eastwards surface jets, the Wyrтки Jets (Wyrтки, 1973). This leads to annual mean westerly winds that favour downwelling and the absence of a permanent equatorial undercurrent. This downwelling circulation is characterized by the Ekman flow in the surface and divergent geostrophic flow in the thermocline (Phillips et al., 2024).

90 In the BoB, which forms the north-eastern basin of the Indian Ocean located between 05°-23°N and 80°-95°E (Fig. 2), the changing monsoon wind system leads to seasonal reversing ocean surface currents and - because of the monsoonal rainfall - a maximum discharge of river systems draining in the BoB such as the Ganges/Brahmaputra and Irrawaddy during the summer monsoon (Tomczak and Godfrey, 1994). The large amount of fresh-water input from these rivers ($1.6 \cdot 10^{12} \text{ m}^3 \text{ yr}^{-1}$; Sarma et al., 2016) causes a permanent decrease of the salinities in surface waters of the northern and central BoB. High surface temperatures further contribute to large upper-ocean stratification that restricts vertical mixing. This leads to nutrient depletion and thus oligotrophic conditions in surface waters of the BoB (e.g. Kumar et al., 2004; Rao et al., 1994; Sarma, 2002; Shetye, 95 1993).

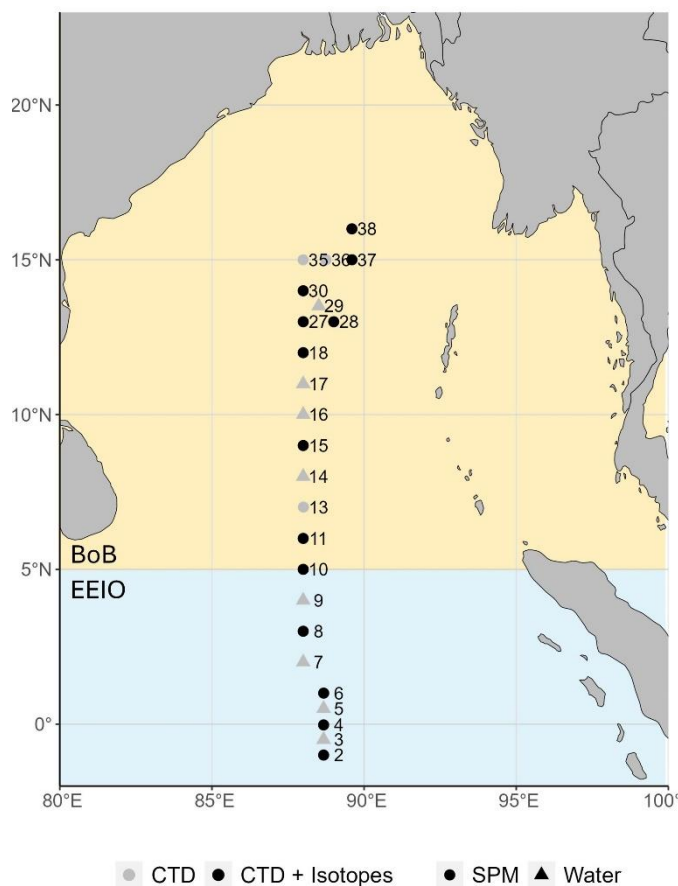


Figure 2: Station location sampled in the EEIO and BoB in April and May 2024. The blue background highlights the EEIO (<math><5^{\circ}\text{N}</math>) and the orange background the BoB (>math>>5^{\circ}\text{N}</math>). Stations shown in grey where CTD and nutrient measurements were conducted. Stations marked in black additionally include nitrate stable isotope sample collection. Suspension samples for particulate nitrogen measurements were done at stations marked with points.

2.2 Sampling

During the research cruise SO305 BIOCAT-IIOE2 (10 April – 22 May 2024; from Colombo (Sri Lanka) to Singapore), full depth CTD casts were performed at 26 stations onboard of the R/V Sonne (Fig. 2). The CTD measurements were carried out with a Seabird CTD system that was equipped with a pressure sensor and with two parallel sensor sets for conductivity (salinity), temperature, and oxygen. Niskin bottles were attached to the CTD to sample the water column at selected water depths. Seawater samples were collected to calibrate the oxygen and conductivity sensors and to measure nutrient concentrations and nitrate stable isotope composition. For nutrients, a full water column profile was sampled at every station. Nitrate stable isotope samples were collected at 13 stations and particulate nitrogen concentrations at 16 stations (Fig. 2).

Oxygen concentrations were measured with SBE 43 Dissolved Oxygen Sensors (Seabird Scientific) and were calibrated with oxygen measurements from discrete water samples applying the Winkler titration method (Hansen, 1999; Winkler, 1888). For

the calibration a linear correction polynomial depending on pressure, temperature and the actual oxygen value was fitted. The uncertainty of the CTD oxygen sensor calibration was determined to a r.m.s. of $\pm 0.8 \mu\text{mol kg}^{-1}$. However, with the Winkler titration method, oxygen concentrations below about 2 to 3 $\mu\text{mol kg}^{-1}$ are not detectable and oxygen concentrations below about 3 $\mu\text{mol kg}^{-1}$ could not be measured with the CTD oxygen sensor.

115 Salinity measurements from the Seabird CTD were calibrated against discrete water samples. Sample salinities were measured using Optimare Precision Salinometers and the calibration was derived following GO-SHIP Repeat Hydrography Manual recommendations (Kawano, 2010) resulting in an accuracy of the calibrated CTD salinities of approximately $\pm 0.002 \text{ g kg}^{-1}$.

2.3 Nutrient analysis

Nutrient concentrations (nitrate, nitrite, silicate and phosphate) were analysed on board using a continuous flow analyzer (CFA, SEAL Analytical) using standard colorimetric methods (Hansen and Koroleff, 1999). Dissolved ammonium concentrations were measured with the ortho-phthalaldehyde (OPA) fluorometric method following Holmes et al. (1999). The detection limits were 0.015 μM for NO_3^- , 0.004 μM for NO_2^- , 0.065 μM for NH_4^+ , 0.013 μM for PO_4^{3-} and 0.025 μM for SiO_2 . We calculated nitrogen deficits (N_{def}) according to Bristow et al. (2017):

$$N_{\text{def}} = [NO_x^-] - \left(\frac{N}{P}\right)_{\text{deep}} \times [PO_4^{3-}] \quad (1)$$

Where, NO_x^- is the sum of nitrate and nitrite concentrations, $(N/P)_{\text{deep}}$ is the average ratio between NO_x^- to phosphate (PO_4^{3-}) in the deepest water samples of each station ranging between 2500 to 4500 m, which was 14.16 during the cruise, and PO_4^{3-} is the phosphate concentration.

Particulate nitrogen sampling was conducted at 5 to 9 different water depths at each suspension station (Fig. 2). Approximately 30 L of sea water were filtered on pre-combusted (450 °C, overnight) Whatman GF/F filters and dried at 40°C for 48 hours. Dried filters were used to determine suspended particulate matter and particulate nitrogen concentrations. For the measurements of particulate nitrogen a laboratory hole puncher was used to extract defined pieces from the filter (punch area: 20.43 mm²). These were measured using an Elemental Analyzer (Euro Vector EA 3000) calibrated against a certified acetanilide standard (IVA Analysentechnik, Germany). The standard deviation was 0.005 % for nitrogen.

2.4 Nitrate stable isotope analysis

For the determination of nitrate stable isotope signatures, water samples were filtered (GF+SFCA, MINISART, 0.45 μm) on board and stored frozen (-20 °C) in Falcon PE (polyethylene) tubes until analysis in the home lab. The samples were shipped as frozen airfreight to Germany. NO_x^- stable isotopes were measured using the denitrifier method (Casciotti et al., 2002; Sigman et al., 2001). NO_x^- in the filtered water sample was reduced to nitrous oxide by *Pseudomonas aureofaciens* (ATCC#13985). The produced nitrous oxide was analysed by a GasBench II coupled with an isotope ratio mass spectrometer (Delta Plus XP, Thermo Fisher Scientific). For calibration, two international standards (USGS34: $\delta^{15}\text{N-NO}_3^- = -1.8 \text{ ‰}$, $\delta^{18}\text{O-NO}_3^- = -27.9 \text{ ‰}$

140 and IAEA: $\delta^{15}\text{N-NO}_3^- = +4.7 \text{ ‰}$, $\delta^{18}\text{O-NO}_3^- = +25.6 \text{ ‰}$) and one internal standard ($\delta^{15}\text{N-NO}_3^- = +7.6 \text{ ‰}$, $\delta^{18}\text{O-NO}_3^- = +24.4 \text{ ‰}$) were measured in each run. The standard deviation for standards and samples was usually $< 0.2 \text{ ‰}$ for $\delta^{15}\text{N-NO}_3^-$ and $< 0.5 \text{ ‰}$ for $\delta^{18}\text{O-NO}_3^-$. Nitrite was usually below the detection limit, leading to the assumption that NO_x^- isotopes are representative for NO_3^- isotopes. If nitrite concentration exceeded 5 %, it was removed prior to analysis using sulfamic acid (Granger and Sigman, 2009), to get nitrate isotope signatures.

145 Nitrite can significantly influence the measured $\delta^{18}\text{O-NO}_3^-$, even if nitrite is present in seawater at very low concentrations. During bacterial conversion to N_2O , nitrite undergoes a smaller fractional loss of oxygen atoms compared to nitrate, leading to lower oxygen isotopic fractionation during nitrite reduction to N_2O (about 25 ‰ less) than when N_2O is generated from nitrate with the same initial $\delta^{18}\text{O}$ (Casciotti and McIlvin, 2007). As a result, calibrating measured oxygen isotope ratios to nitrate reference materials leads to an underestimation of the $\delta^{18}\text{O}$ of NO_3^- . To account for this methodological bias, we
 150 corrected the $\delta^{18}\text{O}$ of NO_3^- by using the measured nitrite concentration relative to that of NO_3^- for each sample. The $\delta^{18}\text{O}$ data for NO_3^- presented these corrected values (Fawcett et al., 2015; Peng et al., 2018).

In the deep ocean, nitrate is produced through nitrification, which utilizes ambient water as the main source of oxygen atoms (Buchwald et al., 2012; Casciotti et al., 2002, 2010). Consequently, changes in the $\delta^{18}\text{O}$ of seawater are reflected in the $\delta^{18}\text{O}$ of the produced nitrate. To account for this, we corrected the $\delta^{18}\text{O}$ for the salinity-driven depth variations in seawater $\delta^{18}\text{O}$
 155 ($\delta^{18}O_{\text{NO}_3, \text{sal corrected}}$), following the method outlined by Knapp et al. (2008):

$$\delta^{18}O_{\text{NO}_3, \text{sal corrected}} = \delta^{18}O_{\text{NO}_3} - 0.16 (\text{sal} - \text{sal}_{1000\text{m}}) \quad (2)$$

Where, $\delta^{18}O_{\text{NO}_3}$ denotes the measured values with nitrite correction, *sal* is salinity of the sample, and $\text{sal}_{1000\text{m}}$ is the salinity in 1000 m depth at each station. The factor 0.16 is the approximate slope between seawater $\delta^{18}\text{O}$ and salinity for the Indian Ocean (LeGrande and Schmidt, 2006).

We calculated nitrate isotopic anomalies $\Delta(15,18)$ according to Sigman et al. (2005):

$$\Delta(15,18) = (\delta^{15}\text{N} - \delta^{15}\text{N}_{\text{deep}}) - \frac{^{15}\epsilon}{^{18}\epsilon} (\delta^{18}\text{O} - \delta^{18}\text{O}_{\text{deep}}) \quad (3)$$

160

Where $\delta^{15}\text{N}$ and $\delta^{18}\text{O}$ are nitrate isotopes of the sample and $\delta^{15}\text{N}_{\text{deep}}$ and $\delta^{18}\text{O}_{\text{deep}}$ the deep water values for each station. The isotopic effects (ϵ) for denitrification are equal so that $^{15}\epsilon/^{18}\epsilon$ equals 1 if no other process is involved.

The $\delta^{15}\text{N}$ of nitrite was calculated via an isotopic mass balance:

$$\delta^{15}\text{NO}_2^- = \frac{\delta^{15}\text{NO}_x^- \times [\text{NO}_x^-] - \delta^{15}\text{NO}_3^- \times [\text{NO}_3^-]}{[\text{NO}_2^-]} \quad (4)$$

Where $\delta^{15}\text{NO}_2^-$, $\delta^{15}\text{NO}_x^-$ and $\delta^{15}\text{NO}_3^-$ are the nitrate isotopes of nitrite, sum of nitrite and nitrate and nitrate, respectively.

3.1 Nutrient distribution

Surface waters (< 50 m) were depleted in nutrients, with nitrate often below the detection limit (Fig. 3a, k), leading to an average nitrate concentration of $0.7 \mu\text{mol L}^{-1} \pm 2.3 \mu\text{mol L}^{-1}$. With depth, nitrate concentrations increased with highest concentrations at ~900 m (maximum values of $38.5 \mu\text{mol L}^{-1}$ at station 28). With further depth it decreased to average bottom water concentrations of $34.9 \pm 0.7 \mu\text{mol L}^{-1}$.

Phosphate concentration followed a similar pattern, with lowest values in surface waters and increased to a maximum of $2.9 \mu\text{mol L}^{-1}$ also observed 900 m (station 28). In bottom waters, phosphate levels declined slightly to an average of $2.5 \pm 0.1 \mu\text{mol L}^{-1}$ (Fig. 3b, l). Silicate concentrations increased with depth, starting from low surface values and reaching average bottom water concentrations of $133.7 \pm 20.6 \mu\text{mol L}^{-1}$ (Fig. 3c, m)

A small nitrite maximum existed at ~70 m with maximum values $>1 \mu\text{mol L}^{-1}$ (Fig. 3 d, n). At the same depth, a small increase in ammonium concentrations was measured up to $0.4 \mu\text{mol L}^{-1}$ (Fig. e, o). Otherwise, nitrite and ammonium were low and often below the detection limit.

The calculated N_{def} was highest in the upper 300 m, peaking at $-3.7 \mu\text{mol L}^{-1}$ at 111 m at station 36. Below ~100 m, the N_{def} reduced to ~350 m, reaching a maximum nitrogen excess of $+1 \mu\text{mol L}^{-1}$. Below 350 m, the N_{def} increased again down to 1000 m, before decreasing once more to approach $\sim 0 \mu\text{mol L}^{-1}$ in the deeper water layers (Fig. 3 h, r). It is striking that station 2 (1°S und 88.40 °E) exhibited NO_x excess up to $2.6 \mu\text{mol L}^{-1}$ at 1000 m depth, whereas all the other stations showed a deficit at the same depths (Fig. 3h). This anomaly seems to be primarily driven by unusually low phosphate concentrations between 500 and 3000 m at station 2 (Fig. 3b), while nitrate profiles remain largely consistent with those at adjacent stations (Fig. 3a). Although hydrological boundaries and biological turnover are unlikely explanations, and no clear evidence for measurement error was found, the cause of this deviation remains unclear.

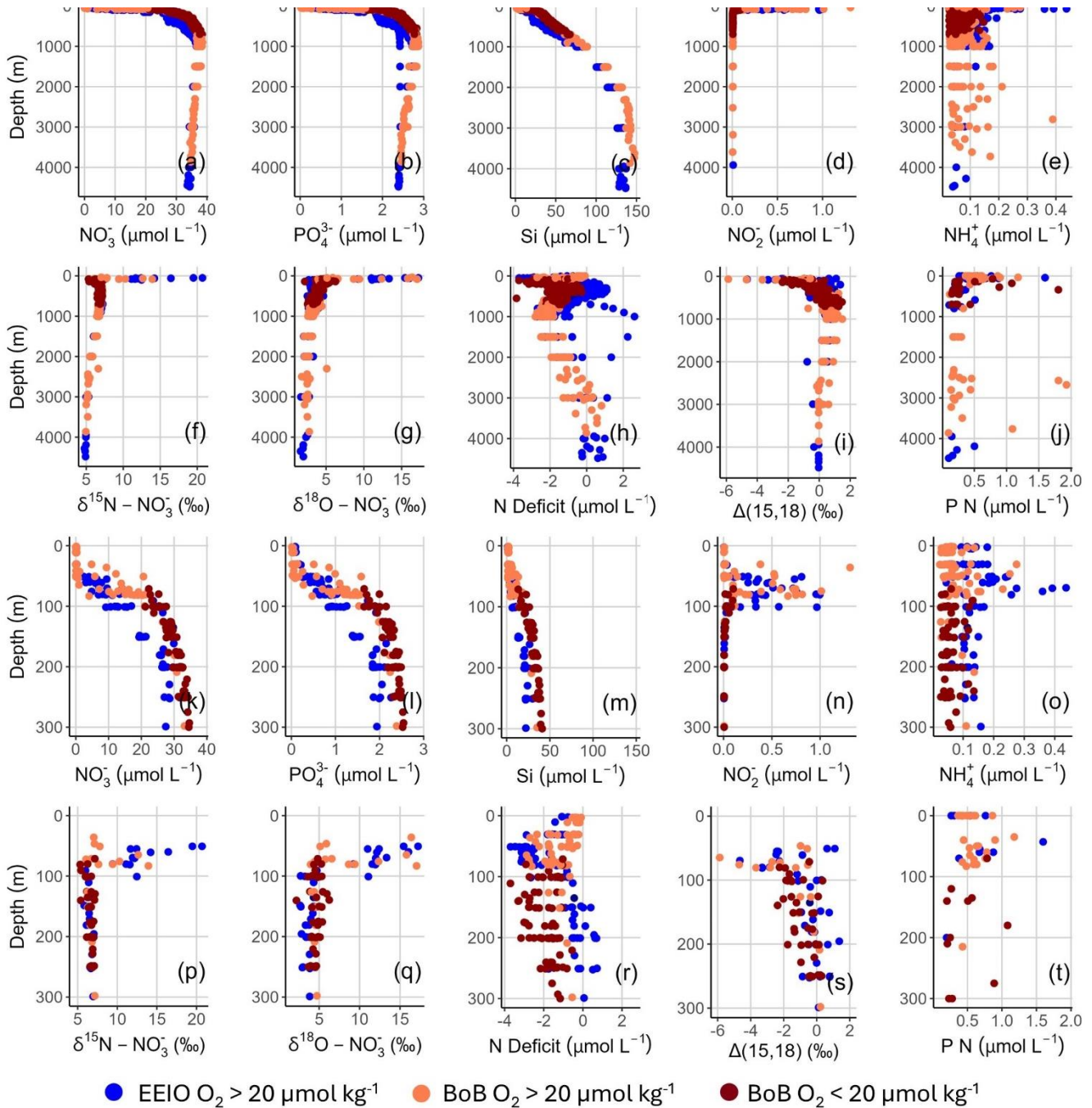
Particulate nitrogen concentrations were low, ranging between 0.1 and $1.9 \mu\text{mol L}^{-1}$ with highest concentrations in the upper 100 m of the water column (Fig. 3j, t). High particulate nitrogen concentrations in deep water were measured at station 37 at 2573 m and 2678 m with $1.8 \mu\text{mol L}^{-1}$ and $1.9 \mu\text{mol L}^{-1}$, respectively, as well as station 35 at 340 m with $1.8 \mu\text{mol L}^{-1}$.

3.2 Nitrate stable isotope distribution

The nitrate stable isotopes showed distinct depth profiles (Fig. 3f, g). Heaviest isotope signatures were measured in the shallowest samples reaching values up to 20.7 ‰ for $\delta^{15}\text{N-NO}_3^-$ and 17.2 ‰ for $\delta^{18}\text{O-NO}_3^-$ (Fig. 3p, q). With increasing water depths, isotopic values decreased to 5.3 ‰ at 80 m depth ($\sigma_\theta = 23.5 \text{ kg m}^{-3}$, station 18) and 2.6 ‰ at 150 m depth ($\sigma_\theta = 25.4 \text{ kg m}^{-3}$, station 4) for $\delta^{15}\text{N-NO}_3^-$ and $\delta^{18}\text{O-NO}_3^-$, respectively. From 150 to 200 m, nitrate isotopes increased. Below 200 m ($\sigma_\theta \sim 27.5 \text{ kg m}^{-3}$), $\delta^{15}\text{N-NO}_3^-$ showed little variability, averaging $6.7 \pm 0.3 \text{ ‰}$. Below 1000 m, $\delta^{15}\text{N-NO}_3^-$ declined, approaching average deep-water values of 5 ‰ (Sigman et al., 2000). $\delta^{18}\text{O-NO}_3^-$ displayed greater variability, especially in more shallow samples, with notably enriched $\delta^{18}\text{O-NO}_3^-$ values observed towards the north. Greatest spatial variation occurred

at approximately 150 m water depth, with samples collected in the south being depleted in $\delta^{18}\text{O}-\text{NO}_3^-$ and samples in the north enriched in $\delta^{18}\text{O}-\text{NO}_3^-$, ranging from 2.6 ‰ at station 4 to 6.2 ‰ at station 38. In deep waters $\delta^{18}\text{O}-\text{NO}_3^-$ approached 5 ‰.

The calculated $\Delta(15,18)$ anomalies were negative in shallow waters (>2 ‰). The anomalies increased with water depth, leading to positive values at depths of 300 to 3000 m and approached 0 ‰ in deep waters (Fig. 3i, s).



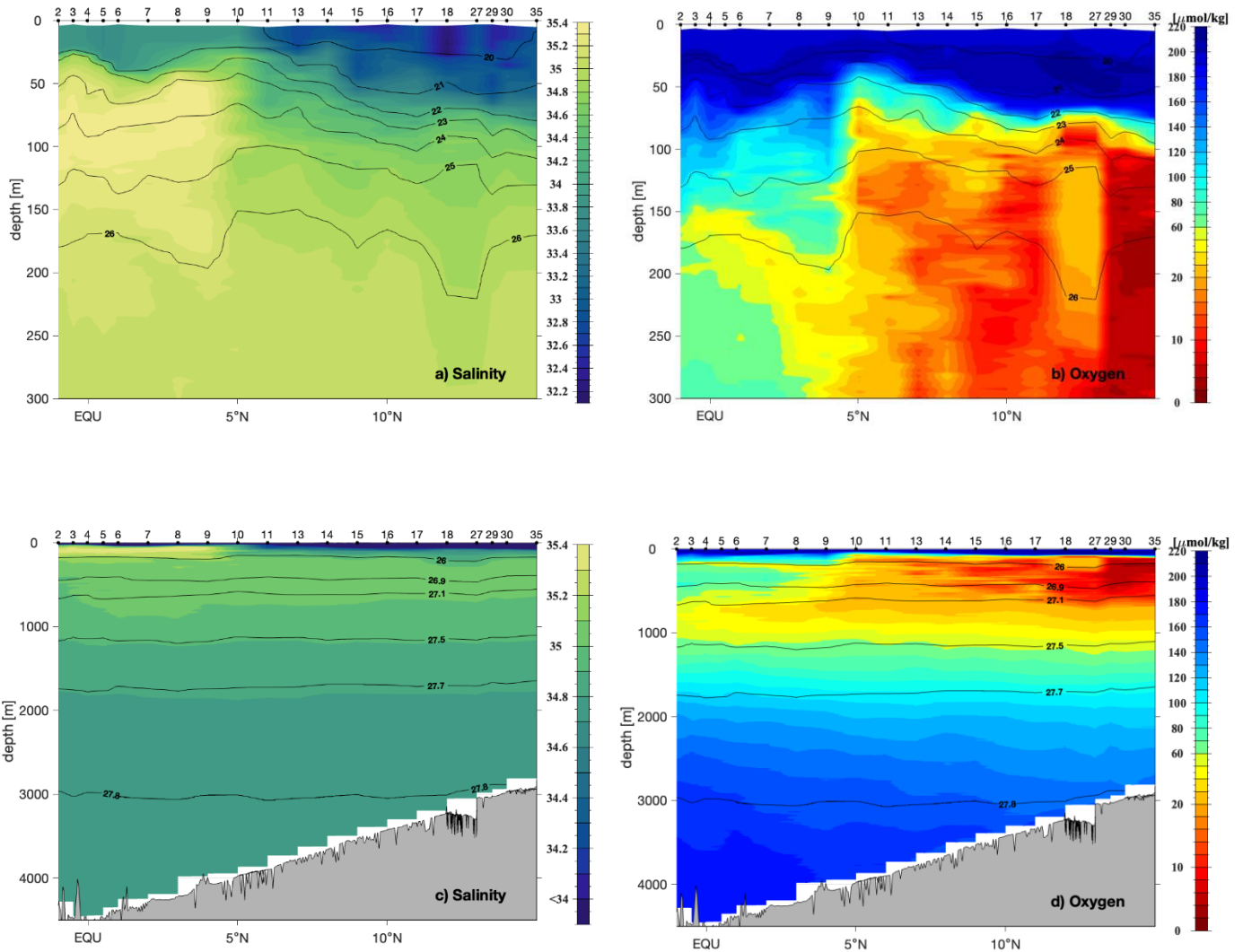
205 **Figure 3: Depth profiles for concentration of nitrate for (a) 0-4500 m, (k) 0-300m, concentration of phosphate for (b) 0-4500 m, (l) 0-300m, concentration of silicate for (c) 0-4500 m, (m) 0-300m, concentration of nitrite for (d) 0-4500 m, (n) 0-300m, concentration of ammonium for (e) 0-4500 m, (o) 0-300m, $\delta^{15}\text{N-NO}_3^-$ for (f) 0-4500 m, (p) 0-300m, $\delta^{18}\text{O-NO}_3^-$ for (g) 0-4500 m, (q) 0-300m, N_{def} for (h) 0-4500 m, (r) 0-300 m, $\Delta(15,18)$ anomalies for (i) 0-4500m, (s) 0-300m, and particulate nitrogen concentrations for (j) 0-4500 m and (t) 0-300 m. Colours indicate regions (blue points for EEIO $< 5^\circ\text{N}$ and orange points for BoB $> 5^\circ\text{N}$, Fig. 2). Samples within the BoB with oxygen concentration $< 20 \mu\text{mol kg}^{-1}$ are displayed as dark red points.**

3.3 Physical water column properties

210 The thermocline waters along the $\sim 88^\circ\text{E}$ section showed a strong separation of the water properties in salinity and oxygen (Fig. 4 a, b). North of 5°N , the upper 80 m were characterized by low salinities < 34 and high temperatures $> 27^\circ\text{C}$. South of 5°N , a salinity maximum of > 35.3 was observed below the surface layer ($\sigma_\theta > 22.7 \text{ kg m}^{-3}$) in water depths of 70 to 120 m and was carried northwards up to $\sim 5^\circ\text{N}$. In deeper water layers (water depth ~ 100 to 580 m, $\sigma_\theta \sim 24.5$ to 27.1 kg m^{-3}), we observed decreasing salinities in the south and increasing salinities in the north. At $\sim 580 \text{ m}$ ($\sigma_\theta \sim 27.1 \text{ kg m}^{-3}$) salinities in both regions were comparable (~ 35), followed by a small decrease in deeper waters (Fig. 4a, c).

215 The surface water ($< 90 \text{ m}$) was saturated in oxygen, and oxygen concentrations decreased with water depth. North of 5°N an oxygen minimum zone existed in 100 to 750 m with oxygen concentrations $< 20 \mu\text{mol kg}^{-1}$, reaching minimum values below the detection limit of $3 \mu\text{mol kg}^{-1}$ in 120 to 220 m water depth. In the south, oxygen concentrations decreased to $\sim 50 \mu\text{mol kg}^{-1}$. At $\sim 400 \text{ m}$ ($\sigma_\theta \sim 26.9 \text{ kg m}^{-3}$) an oxygen peak was measured from 1°S to 6°N . Followed by a low oxygen water mass below 580 m ($\sigma_\theta \sim 27.1 \text{ kg m}^{-3}$). In deep waters oxygen concentrations increased again to $150 \mu\text{mol kg}^{-1}$ (Fig. 4b, d).

220



225 **Figure 4: Vertical distribution of (a, c) salinity and (b, d) oxygen in $\mu\text{mol kg}^{-1}$ in the upper 300 m depth (a, b) and in the entire water column along the $\sim 88^\circ\text{E}/88.7^\circ\text{E}$ section from CTD measurements during SO305 in April and May 2024. Potential density surfaces are contoured in black. Black dots and numbers denote the ship station numbers (also shown in Fig. 2).**

3.4 Water mass distribution

Water masses were characterized by their potential temperature (T), salinity (S), density, and oxygen concentration profiles.

230 The T-S diagram (potential temperature versus salinity) for this study allowed to identify two different, clearly separated, identifiable water mass distributions within the study area (Fig. 5a): the EEIO south of 5°N and the BoB north of 5°N . The T-S profiles diverge in two distinct branches in the mixed layer and in the thermocline below σ_θ values of approximately

27 kg m⁻³, with higher salinity water masses observed in the EEIO and low-salinity water masses found in the BoB (Fig. 5a). The same separation was identified in the σ_θ vs salinity (Fig. 5b) and σ_θ vs oxygen plots (Fig. 5c). Only one station at 5°N showed mixing between water masses of the BoB and EEIO (Fig. 5a und b), indicating that exchange of water masses between the BoB and southern hemisphere is limited due to the blocking effect of the equatorial current system (Schott and McCreary, 2001).

In the Bay of Bengal (>5 °N), T-S diagrams were largely consistent with previous studies (Fig. 5a; Emery, 2001; Rahman et al., 2021; Sengupta et al., 2013; Tomczak and Godfrey, 1994), which identified the following water masses in the BoB: 1) Bay of Bengal Water (BoBW), 2) Mixed Zone (MZ), 3) Indonesian Throughflow (ITF), 4) Indian Central Water (ICW), 5) Indian Deep Water (IDW) and 6) Circumpolar Deep Water (CDW).

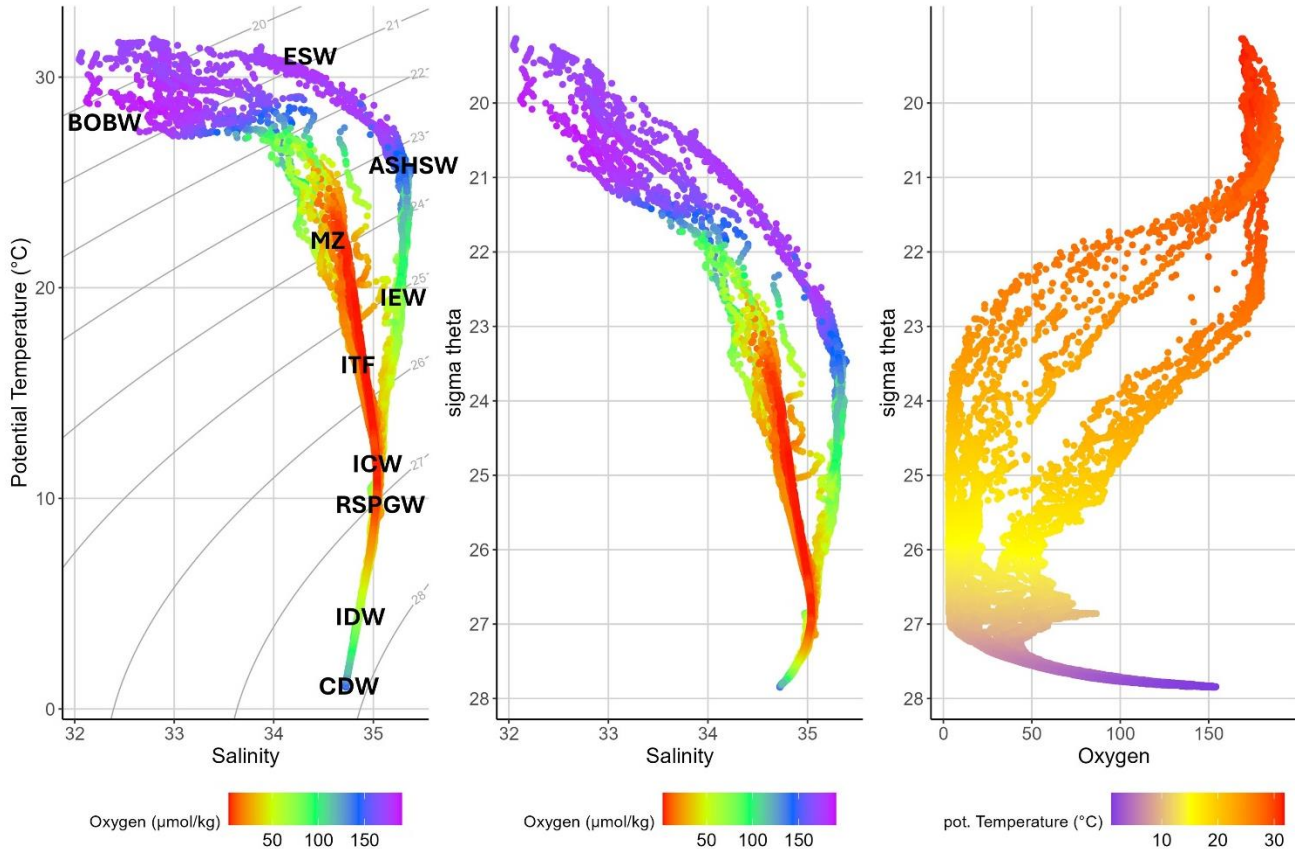
The BoBW in the near surface water of the BoB is characterized by extremely low salinities ($S < 33.5$) due to the large amount of freshwater input through the combination of strong river discharge and excess precipitation (Schott and McCreary, 2001). Further, other studies detected Arabian Sea High Salinity Water (ASHSW) and Red Sea Persian Gulf Water (RSPGW) in the BoB (Jain et al., 2017; Rahman et al., 2021; Sheehan et al., 2020) (Fig. 5a). The ASHSW spreads eastward in the upper 100 m depth with the Southwest Monsoon Current (SMC) around the southern tip of Sri Lanka during summer and northward into the BoB with the East India Coastal Current (EICC) and slides below the BoBW (Vinayachandran et al., 1999). Our measurements in the BoB did not show the presence of ASHSW north of 5°N, possibly because our cruise took place during the spring transition phase. This aligns with Jain et al. (2017), who found that ASHSW disappears to the east and north of the south-central bay (85°E, 8°N) as a result of mixing with the BoB's fresher surface waters. Maximum salinity across most of the BoB is attributed to Red Sea Persian Gulf Water (RSPGW). There is still discussion about the extension of Persian Gulf Water and Red Sea Water into the BoB. Nonetheless, the presence of RSW and PGW in the BoB has been previously shown by Jain et al. (2017) and Sheehan et al. (2020) (Fig. 5a).

The BoB thermocline waters of the upper 1000 m depth mainly originate from southern hemisphere due to the geographical boundary in the north. The thermocline waters primarily consist of ICW and water originating from the ITF (You and Tomczak, 1993). The ITF brings relatively low salinity water ($S < 34.6$) originating from the tropical Pacific Ocean and merges with the South Equatorial Current (SEC) on its way to the western boundary (Gordon, 2005; Sprintall et al., 2009; You, 1997). ICW is formed along the subtropical convergence zone by subduction and is carried westward by the SEC (Sprintall and Tomczak, 1993; You, 1997). ICW is characterized by higher salinity waters ($S > 35$, Fig. 5a) and a quasi-linear relation above 7 °C (Schott and McCreary, 2001; Sverdrup et al., 1942). During the summer monsoon, both water masses cross the equator and flow into the Arabian Sea and eventually in the BoB (Schott et al., 2009; Tomczak and Godfrey, 1994; You, 1997).

In the thermocline waters of the EEIO, we identified the presence of equatorial surface water (ESW), ASHSW, Indian Equatorial Water (IEW), and RSPGW. The IEW mainly consists of ITF with contributions of ICW (Tomczak and Godfrey, 1994). The observed separation between BoBW and ESW at 5°N aligns with findings by Junior (2023), who identified ESW between 10°S and 5°N, extending westwards from 60°E. Shee et al. (2023) assigned the most upper 50 m with low salinities to BoBW with ESW being present from 50-100 m. However, in our observation, the pronounced salinity maximum between

σ_θ 23 and 24 kg m^{-3} shows the presence of ASHSW at water depths between 35-90 m, contrasting the absence of this water mass in the BoB (Fig. 5a).

IDW originates from North Atlantic Deep Water, which is transported into the Indian Ocean with the Circumpolar Current and spreads northward along the western boundary (Tomczak and Godfrey, 1994). IDW can be found below about $\sigma_\theta=27.6$ $\mu\text{mol kg}^{-1}$ with oxygen values between 100 and 200 $\mu\text{mol kg}^{-1}$ ventilating the thermocline from below (Ditkovsky et al., 2023). CDW can be found just below the IDW with a salinity of about $S=34.7$ and very low temperature (Schott and McCreary, 2001).



275 **Figure 5: (a) T-S (potential temperature versus salinity) diagram from CTD measurements with marked water masses. The colour bar indicates oxygen concentrations in $\mu\text{mol kg}^{-1}$, grey lines indicate density surfaces in σ_θ in kg m^{-3} . (b) Sigma-theta in kg m^{-3} plotted against salinity diagram with colour bar indicating oxygen concentrations in $\mu\text{mol kg}^{-1}$. (c) Sigma-theta in kg m^{-3} plotted against oxygen in $\mu\text{mol kg}^{-1}$ with colour bar indicating potential temperature in $^\circ\text{C}$. Abbreviations: Bay of Bengal Water (BOBW), Equatorial Surface Water (ESW), Arabian Sea High Salinity Water (ASHSW), Mixed Zone (MZ), Indian Equatorial Water (IEW), Indonesian Throughflow Water (ITF), Indian Central Water (ICW), Red Sea Persian Gulf Water (RSPGW), Indian Deep Water (IDW) and Circumpolar Deep Water (CDW).**

280

3.4 Correlation analysis

We examined the relationship of nitrate isotopes with salinity, potential temperature, and multiple regressions analysis of both isotopes using salinity and potential temperature (see supplementary material). A strong correlation of isotope changes with water mass tracers generally suggests that water masses are the main drivers of change, whereas a lack of correlation implies additional processes. Isotopic variability showed no strong correlation in either BoB or EEIO when data from all depths were analysed (best fit with multiple regression analysis: $R^2 < 0.24$, $p < 0.001$ and $R^2 < 0.58$, $p < 0.001$ for $\delta^{15}\text{N-NO}_3^-$ and $\delta^{18}\text{O-NO}_3^-$, respectively, in BoB and $R^2 < 0.47$, $p < 0.001$ and $R^2 < 0.52$, $p < 0.001$ for $\delta^{15}\text{N-NO}_3^-$ and $\delta^{18}\text{O-NO}_3^-$ in EEIO). This indicates that water mass changes are not the sole driver for isotopic variability within the entire water column. The correlations improved significantly after excluding the upper water masses from both regions. In the BoB, removing the measurements done in BoBW and MZ from the dataset (water depth from 0 – 170 m), led to strong significant correlations for both $\delta^{15}\text{NO}_3^-$ (best fit with multiple regression analysis: $R^2 = 0.84$, $p < 0.001$) and $\delta^{18}\text{O-NO}_3^-$ (best fit with potential temperature: $R^2 = 0.65$, $p < 0.001$), which further improved by excluding measurements from the ITF (best fit with multiple regression analysis: depths to 300 m, $R^2 = 0.89$, $p < 0.001$ and $R^2 = 0.61$, $p < 0.001$ for $\delta^{15}\text{N-NO}_3^-$ and $\delta^{18}\text{O-NO}_3^-$, respectively). In the EEIO, excluding measurements from the ESW, ASHSW and IEW (0 – 225 m water depth) led to strong significant correlations (best fit with multiple regression analysis: $R^2 = 0.84$, $p < 0.001$ and $R^2 = 0.55$, $p < 0.001$ for $\delta^{15}\text{N-NO}_3^-$ and $\delta^{18}\text{O-NO}_3^-$), respectively.

4 Discussion

4.1 Correlation analysis

The nitrate stable isotopes exhibited distinct depth profiles, with significant variation in the upper 300 m and minimal variation at greater depths. In the deepest samples, $\delta^{15}\text{N-NO}_3^-$ declines, approaching average deep-water values of 5 ‰ (Sigman et al., 2000). These isotopic changes can result from changes of in-situ nitrogen turnover processes as well as changes in water masses. For the latter case, nitrogen concentration and isotope signatures are not due to processing in the BoB but are inherited from the region of water mass formation and are transported to the study site (e.g. Harms et al., 2019; Marshall et al., 2023). To evaluate the extent to which variations in nitrate stable isotopes can be attributed to changes in water mass contribution, we examined the relationship of nitrate isotopes with salinity and potential temperature (section 3.5), showing that water masses are not the sole driver for isotopic variability with no strong correlation in either BoB or EEIO when data from all depths were analysed. Excluding water masses in the upper 200 to 300 m of the water column improved the correlations significantly, leading to strong significant correlations of water mass tracers with dual nitrate stable isotopes. Therefore, we conclude that the $\delta^{15}\text{N-NO}_3^-$ and $\delta^{18}\text{O-NO}_3^-$ in the deeper water were water mass specific and reflect variations in the water mass distributions, while the nitrate isotopic signatures in the upper 300 m were influenced by in-situ nitrate fractionation.

4.2 Nitrate turnover in the upper 300 m of the water column

In the upper 300 m, nitrate isotope depth profiles showed significant variation, with highest values in the uppermost samples, lowest values around 70 – 90 m ($\sigma_0 \sim 22\text{-}24 \text{ kg m}^{-3}$), and a slight increase with greater depth (Fig. 3). A comparison of nitrate stable isotopes in the upper water column between the EEIO and BOB reveals several notable differences: 1) similar $\delta^{15}\text{N-NO}_3^-$ depth profiles in EEIO and BOB with distinct variabilities (Fig. 3p), 2) enriched $\delta^{18}\text{O-NO}_3^-$ in BoB with oxygen concentration below $20 \mu\text{mol kg}^{-1}$ compared to lower values in the oxic EEIO (Fig. 3q, Fig. 6c), and 3) persistent N_{def} between 100 and 300 m ($\sigma_0: 24 - 27 \text{ kg m}^{-3}$) in BoB (Fig. 3r) while in the EEIO the N_{def} is markedly reduced below ~ 100 m. Although some EEIO samples do show N_{def} at depths >100 m, these are significantly less pronounced than in the BoB and likely reflect a NO_3^- source due to coupled remineralisation and nitrification processes counterbalancing the N_{def} . We also acknowledge a potential bias in our N_{def} calculation (equation 1) based on deep-water samples at each station. Applying this deep-water ratio to shallower layers may overestimate the N_{def} in the upper water column, especially if the N/P ratio varies with depth due to biological or physical processes.

Taken together, the vertical and regional patterns in nitrate isotopes and N_{def} suggest distinct nitrate cycling in the BoB and EEIO. The isotopic variations with depth suggest changes in nitrate cycling with depths, while the regional decoupling between $\delta^{15}\text{N-NO}_3^-$ and $\delta^{18}\text{O-NO}_3^-$ shows regional differences in nitrate cycling in the EEIO and BoB.

4.2.1 Surface waters

In the majority of the samples from water depths above ~ 80 m, $\delta^{15}\text{N-NO}_3^-$ and $\delta^{18}\text{O-NO}_3^-$ increased significantly up to $> 20 \%$ and $> 15 \%$, respectively (Fig. 3p, q). We attribute this simultaneous increase in both isotopes along with low nitrate concentrations (Fig. 3k, Fig. 3p, q) in oxic surface waters to nitrate assimilation. Upper ocean assimilation has been observed and documented in numerous studies (e.g. Fawcett et al., 2015; Peng et al., 2018; Wankel et al., 2007). During nitrate assimilation, phytoplankton preferentially utilize the lighter isotopes, resulting in an enrichment of the remaining nitrate pool as its concentration decreases (Fig. 1). Culture studies showed that nitrate assimilation leads to a ratio of $\delta^{18}\text{O}$ to $\delta^{15}\text{N}$ of 0.96-1.09 (Granger et al., 2004, 2010; Karsh et al., 2012), which matches the ratio of 0.95 ($R^2 = 0.70$, $p < 0.01$) found in our study (Fig. 6a). This indicates active phytoplankton uptake as dominant nitrate sink in the surface water of the BoB and EEIO (Fig. 7).

In the warm, sunlit ocean, N_2 fixation may produce newly bioavailable nitrogen (Fig. 1, Marshall et al., 2023). However, in the BoB, Löscher et al. (2020) found no consistent evidence for N_2 fixation, whereas Saxena et al. (2020) detected N_2 fixation but assessed its contribution to primary production as negligible. Shiozaki et al. (2014) only found low N_2 fixation rates in the south and equatorial Indian Ocean, with similar minimal influence on primary production (Saxena et al., 2020). Since $\delta^{15}\text{N-NO}_3^-$ is not significantly more depleted than $\delta^{18}\text{O-NO}_3^-$, which would be typical for N_2 fixation (Marshall et al., 2023), and in agreement with the previous studies (Löscher et al., 2020; Saxena et al., 2020; Shiozaki et al., 2014), N_2 fixation seems negligible in the BoB and EEIO in our study.

In surface waters, another possible nitrogen source is atmospheric deposition that is reflected in low $\delta^{15}\text{N-NO}_3^-$ (-14 ‰ to 2 ‰; Altieri et al., 2021) and high $\delta^{18}\text{O-NO}_3^-$ (>60 ‰; Kendall et al., 2007) values. Thus, the observed simultaneous increase of both nitrate isotopes contradicts significant nitrate input by atmospheric aerosol deposition which is in line with findings of Sarma (2022). SO305 took place during the transition period and the early stage of the southwest monsoon. The prevailing south-westerly winds were, therefore, not favourable for a pronounced aerosol transport from the land and led to low aerosol deposition at the time of our study (Bange et al., 2024).

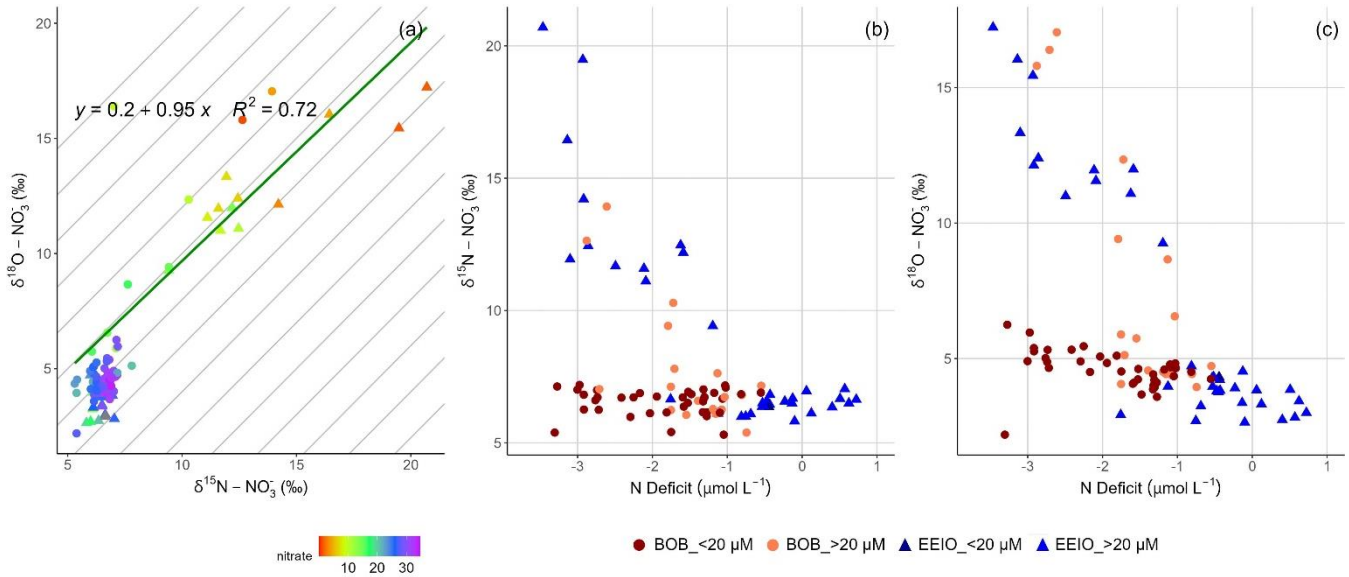


Figure 6: Nitrate isotope signatures and nitrate deficit for samples in the upper 300 m: (a) $\delta^{18}\text{O-NO}_3^-$ plotted against $\delta^{15}\text{N-NO}_3^-$. Regression line, equation and R^2 values was only calculated for surface water samples (<100 m). Diagonal grey lines have a slope of 1. Colours indicate nitrate concentrations and shapes the region of the sample (filled triangles stand for EEIO, full circles stand for BoB). (b) $\delta^{15}\text{N-NO}_3^-$ and (c) $\delta^{18}\text{O-NO}_3^-$ plotted against N_{def} . Colours and shapes indicate region (blue filled triangles stand for EEIO <math><5^\circ\text{N}</math> and orange filled circles stand for BoB >math>5^\circ\text{N}</math>). Filled dark red circles display samples in the BoB with oxygen concentrations <math><20 \mu\text{mol kg}^{-1}</math>.

4.2.2 Subsurface waters

At $\sim 70\text{-}90 \text{ m } \sigma_\theta$: $22 - 24 \text{ kg m}^{-3}$), a nitrite maximum exists with concentrations $> 1 \mu\text{mol L}^{-1}$ (Fig. 3n). Just below the nitrite maximum, lowest nitrate isotopes were measured (Fig. 3p, q) alongside a steep increase in nitrate concentration (Fig. 3k) and reduced N_{def} (Fig. 3r), indicating nitrate production via nitrification. Ammonium was most probably produced via remineralisation of organic material originating either from new production or regenerated production (Fig. 1; Marshall et al., 2023), even though rapid nitrification can disguise this production by immediate oxidation of freshly produced ammonium. Our data (Fig. 6a) is consistent with findings from the Sargasso Sea, where Fawcett et al. (2015) observed changes in $\delta^{18}\text{O-NO}_3^-$ without corresponding shifts in $\delta^{15}\text{N-NO}_3^-$, indicating nitrification alongside partial nitrate assimilation. The decoupling occurs because nitrification produces nitrate with a relatively high $\delta^{18}\text{O}$ values, while its $\delta^{15}\text{N}$ remains like that of organic nitrogen remineralized. At the same time, nitrate assimilation removes lower $\delta^{18}\text{O}$, causing the $\delta^{18}\text{O}$ of the remaining nitrate to increase

more than $\delta^{15}\text{N}$. Additionally, ammonium in the euphotic zone is more likely oxidized than assimilated due to a large isotope effect during ammonium oxidation. This introduces low $\delta^{15}\text{N-NO}_3^-$, further reducing $\delta^{15}\text{N}$ relative to $\delta^{18}\text{O}$ (Fawcett et al., 2015).

370 The formation of the primary nitrite maximum (PNM) at the base of euphotic zone may result from an imbalance between ammonium oxidation and nitrite oxidation when ammonium oxidation is higher than nitrite oxidation. We calculated $\delta^{15}\text{N-NO}_2^-$ via a mass balance. All calculated values were extremely low with an average of -58.1 ‰. Due to the low concentration, the calculation of nitrite isotope is prone to errors. However, values below -14 ‰, as in this case, indicate ongoing nitrite oxidation, which exhibits an inverse kinetic isotope effect (-9 – -20‰; Buchwald and Casciotti, 2010; Casciotti, 2009) and amplifies the ^{15}N depletion of nitrite caused by nitrate reduction (Fig. 1; Casciotti, 2009).

375 The observed $\delta^{18}\text{O-NO}_3^-$ minimum values of 2.6 ‰ and 3.6 ‰ in the EEIO and BoB, respectively, are close to the global mean oceanic value of 2.4 ‰ relative to the nitrification source (Sigman et al., 2009) indicating freshly nitrified nitrate.

Since we did not find any indication of significant N_2 fixation (section 4.2.1), it appears that primarily regenerative nitrate production by nitrification of phytoplankton organic matter takes place in the BoB and EEIO (Fig. 7).

4.2.3 Nitrogen deficit in subsurface waters of the BoB

380 Between 100 and 300 m, the BoB exhibited a significant N_{def} , reaching up to $-3.7 \mu\text{mol L}^{-1}$ (Fig. 3r). Oxygen concentrations in the BoB at depth of the N_{def} were low and fell below $20 \mu\text{M}$, and in some cases oxygen concentrations even dropped below the detection limit of $3 \mu\text{M}$ (Fig. 4b). Such low oxygen concentrations are theoretically favourable for nitrate removal via anammox or denitrification (Bristow et al., 2016; Dalsgaard et al., 2014; Kalvelage et al., 2011; Rixen et al., 2020).

Generally, water column nitrate removal should be accompanied by an isotopic enrichment of nitrate. In the adjacent OMZ of the Arabian Sea, such removal processes result in substantial enrichment of nitrate stable isotopes, with values reaching up to 30 ‰ for both $\delta^{15}\text{N-NO}_3^-$ and $\delta^{18}\text{O-NO}_3^-$ (Gaye et al., 2013; Martin and Casciotti, 2017; Naqvi et al., 1998). Although the isotopic enrichment observed in the BoB is less pronounced, we still detect a significant signal: samples characterized by persistent N_{def} and low oxygen concentrations were accompanied by a small, but notable enrichment of both $\delta^{15}\text{N-NO}_3^-$ and $\delta^{18}\text{O-NO}_3^-$ (Fig. 6b, c). This enrichment clearly differs from nitrate dual isotope signatures in the oxic water column in the BoB and EEIO (Fig 3e, g), providing strong evidence that nitrogen removal processes are indeed active in the BoB.

390 Within the OMZ of the BoB, nitrate stable isotopes reached values up to 7.2 ‰ and 6.3 ‰ for $\delta^{15}\text{N-NO}_3^-$ and $\delta^{18}\text{O-NO}_3^-$, respectively. This corresponds to an enrichment of 1.7 ‰ and 4.1 ‰, respectively, over deep water values. The enhanced enrichment of $\delta^{18}\text{O-NO}_3^-$ in the BoB becomes particularly evident in comparison with the EEIO, where $\delta^{18}\text{O-NO}_3^-$ values were notably lighter (Fig. 3q). Theoretically, a shift in $\delta^{18}\text{O-H}_2\text{O}$ can lead to changes in $\delta^{18}\text{O-NO}_3^-$ of freshly produced nitrate because oxygen from water is incorporated (Kool et al., 2007; Snider et al., 2010). However, BoB and EEIO have similar $\delta^{18}\text{O-H}_2\text{O}$ signatures (Kim et al., 2021; Sengupta et al., 2013; Srivastava et al., 2007). Therefore, we argue that the observed $\delta^{18}\text{O-NO}_3^-$ shift and enrichment in the BoB was not caused by regional $\delta^{18}\text{O-H}_2\text{O}$ differences but is rather caused by differences

in nitrate turnover between BoB and EEIO. Based on the correlation of $\delta^{18}\text{O-NO}_3^-$ increase with N_{def} in the BoB (Fig. 6c), we conclude that the main differences are linked to nitrate loss in the anoxic water column of the BoB.

400 We calculated negative $\Delta(15,18)$ anomalies ranging from -2 ‰ to 0 ‰ (Fig. 3s). An enhanced enrichment of $\delta^{18}\text{O-NO}_3^-$ has been observed in the BoB before (Bristow et al., 2017) and in other OMZs (Gaye et al., 2013; Martin and Casciotti, 2017) and was attributed to coupled anaerobic and aerobic processes, involving nitrate reduction to nitrite followed by its reoxidation to nitrate. Studies have shown that during nitrate reduction, the ratio of the kinetic isotope effect is 1:1 ($^{15}\epsilon:^{18}\epsilon$) (Granger et al., 2008). However, repeated nitrate reduction and nitrite oxidation cause little changes on the isotopic signature of $\delta^{15}\text{N-NO}_3^-$,

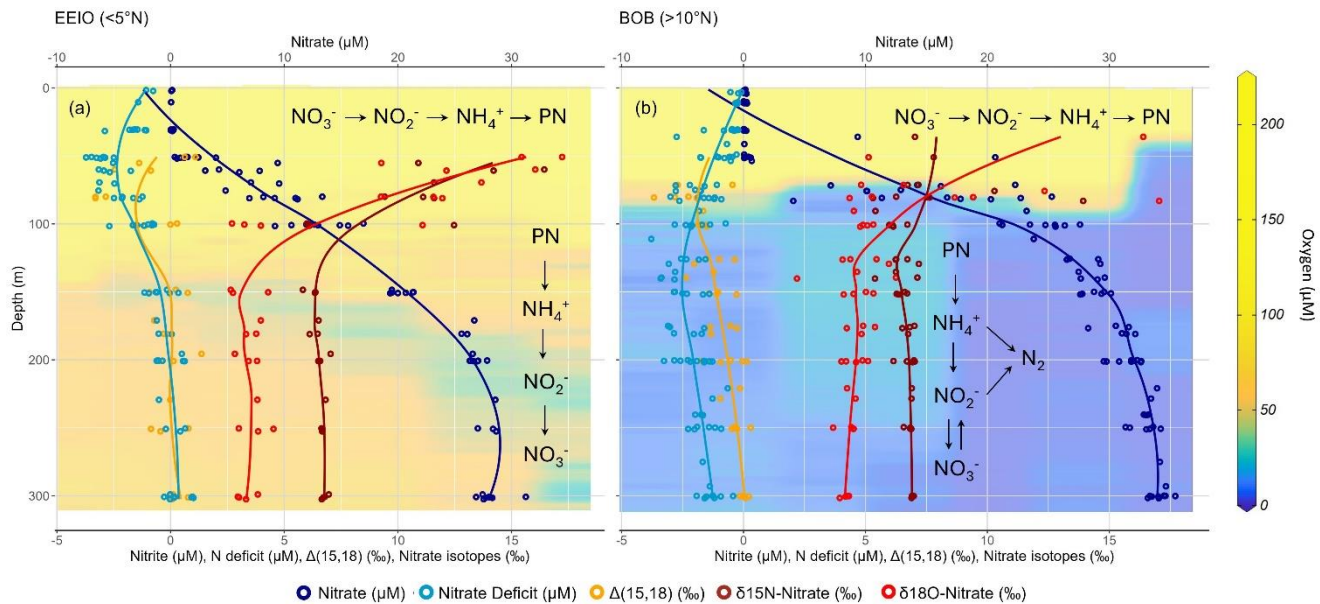
405 but leads to an increase in $\delta^{18}\text{O-NO}_3^-$ values because nitrite oxidation strongly fractionates on nitrogen with -9 ‰ to -20‰ and less on oxygen(-1 ‰ to -8 ‰, respectively (Buchwald and Casciotti, 2010; Casciotti, 2009). The nitrate that undergoes reduction initially has a lower $\delta^{18}\text{O}$ value than the reoxidized nitrite, causing the negative $\Delta(15,18)$ anomaly (Gaye et al., 2013). Thus, in the OMZ of the BoB, the combination of an N_{def} with observed isotopic enrichment might result from ongoing nitrate reduction/reoxidation cycles and partial nitrite consumption of nitrite by anammox (Fig. 7).

410 Bristow et al. (2017) identified a significant potential for nitrogen removal via anammox, with little evidence of denitrification in the BoB. Based on their measurement of oxygen at trace level, they hypothesized that these trace oxygen levels enable nitrite-oxidizing bacteria to outcompete anammox bacteria for available nitrite, leading to nitrite limitation of anammox rather than ammonium or oxygen limitation. Anammox bacteria are known for their tolerance of ambient oxygen levels, with tolerances as high as 20 μM (Okabe et al., 2023), making their contribution to the N_{def} more likely than denitrification.

415 Denitrification, shown to be driven by episodic supply of organic matter (Ward, 2013), might also be limited by low particulate nitrogen availability in the BoB (Fig. 3j, t). Furthermore, Bristow et al. (2017) found a similar isotopic enrichments in nitrate isotopes and negative $\Delta(15,18)$ anomalies that match our data. Thus, anammox appears to be the more plausible nitrogen loss pathway in the BoB. Nitrogen removal by anammox can explain the observed nitrogen deficit as well as the dual isotope enrichment of nitrate.

420 Intriguingly, anammox bacteria can also produce nitrate via re-oxidation of nitrite, as they fix carbon dioxide into biomass using reducing equivalents produced during the oxidation of nitrite to nitrate (Dalsgaard et al., 2003; Kobayashi et al., 2019). The nitrate production via anammox bacteria has a significant impact on nitrite and nitrate dual isotopes, but is still often overlooked (Granger and Wankel, 2016; Kobayashi et al., 2019). Similar to conventional nitrification, nitrite oxidation via anammox has an inverse isotopic effect (Brunner et al., 2013; Kobayashi et al., 2019) with a significant higher isotope effect

425 in $^{15}\epsilon$ ranging from -30 to -45 ‰ than $^{18}\epsilon$ ranging from -2 to -12 ‰ (Kobayashi et al., 2019). Thus, nitrite oxidation by anammox bacteria could contribute to the decoupling of nitrate isotopes and resulting enrichment of $\delta^{18}\text{O-NO}_3^-$, further supporting anammox as the most important nitrogen loss pathway in the OMZ of the BoB.



430 **Figure 7: Schematic overview of nitrogen turnover processes in the (a) EEIO and (b) BoB in the upper 300 m of the water column.** The figure shows individual measurements and moving averages for nitrate ($\mu\text{mol L}^{-1}$), N_{def} ($\mu\text{mol L}^{-1}$), $\Delta(15,18)$ (‰), $\delta^{15}\text{N-NO}_3^-$ (‰) and $\delta^{18}\text{O-NO}_3^-$ (‰) for each region. Nitrate is shown in dark blue, N_{def} in light blue, $\delta^{15}\text{N-NO}_3^-$ in dark red, $\delta^{18}\text{O-NO}_3^-$ in light red and $\Delta(15,18)$ in orange. The background indicates measured oxygen concentrations ($\mu\text{mol kg}^{-1}$). The zone of nitrate assimilation in surface waters is evident by high $\delta^{15}\text{N-NO}_3^-$ and $\delta^{18}\text{O-NO}_3^-$ values as well as low nitrate concentrations and a N_{def} . In the EEIO subsurface water are dominated by coupled remineralisation and nitrification, which shows in a reduced N_{def} and lighter nitrate isotopes. In the BoB, subsurface waters with low oxygen concentrations also show signs of nitrate reduction by a persistent N_{def} below 100 m along with enriched $\delta^{18}\text{O-NO}_3^-$ values that lead to negative $\Delta(15, 18)$ anomalies. This can be explained by nitrate reduction, which might be fuelled by nitrate production during nitrification, coupled with anammox.

5 Conclusions

This study sheds light on the nitrogen cycle in the EEIO and BoB. We used nitrate stable isotope signatures to disentangle turnover processes and reveal fundamental regional differences in nitrogen cycling between both regions. A detailed analysis of water mass distributions in both regions revealed that the OMZ in the BoB was well separated from the EEIO at 5°N . This separation was also reflected in water column distribution of nitrate isotope signatures. Nitrate isotope signatures in deeper water masses (> 300 m) were solely controlled by changes in water mass distribution, whereas in the upper 300 m isotope variations were caused by on-site nitrate fractionation. In surface waters (0-80 m), one active nitrate sink was phytoplankton assimilation, causing a significant isotopic enrichment and N_{def} in the upper 50 m. In the underlying waters, nitrification took place, most presumably fuelled by regenerated phytoplankton biomass rather than by remineralisation of nitrogen that was freshly fixed by N_2 fixation. In the OMZ of the BoB between 100 and 300 m, we found a persistent N_{def} along with nitrate isotope signatures that were slightly but significantly enriched compared to deep water values and samples from the same depths in the EEIO. Given the dynamic oxygen concentrations in the water column (Bristow et al., 2017; Johnson et al., 2019), anammox appeared to be the more plausible nitrogen loss pathway in the BoB. Overall, we find that there is convincing

evidence for nitrate reduction processes in the BoB. To fully assess the significance of nitrogen loss in the Bay of Bengal and the potential future evolution of nitrate reduction pathways, it is essential to conduct detailed studies on nitrogen cycling processes, measure the rates of potential nitrogen loss mechanism, and explore the microbial communities that drive these transformations within this dynamic and ecological significant oxygen minimum zones.

455 **Data availability**

SO305 BIOCAT-IIOE2 datasets (<https://www.pangaea.de/?q=campaign%3A%22SO305%22>, last access: 24.06.2025), along with the nitrate isotope data set (<https://doi.org/10.1594/PANGAEA.983257>) are available on PANGAEA (Felden et al., 2023).

Author contributions

GS and BG designed this study. HWB was the principal investigator during SO305 BIOCAT-IIOE2, GS took the nitrate stable
460 isotopes samples and RC was responsible for CTD operations. JP and GS measured the nitrate stable isotope samples. KD, TS, JP, HWB, RC and BG contributed with scientific and editorial recommendations. GS wrote the manuscript and prepared the submitted paper with contributions from all co-authors.

Competing interest

At least one of the (co-)authors is a member of the editorial board of Biogeosciences. The authors have no other competing
465 interests to declare.

Acknowledgements

We thank the captain and crew of the R/V SONNE for their support during SO305 BIOCAT-IIOE2, Dr. Niko Lahajnar for his support with cruise logistics, Tjark Andersch and Leandro Nazzari for their support during the cruise, Ramazan Cetin for measuring particulate nitrogen content, Kira Lange, Leon Schmidt and Jannis Usinger for measuring the nutrient and oxygen
470 concentrations as well as the entire CTD team for operating the CTD and water samples on board. We also highly appreciate the scientific feedback we received from Bo Thamdrup and Victor Fernandez Juarez.

Data was visualized by R, specifically ggplot2 (version 3.4.1; Wickham et al., 2016) and ggpubr (version 0.6.0; Kassambara, 2023). The map of our study area was plotted using rnatualearth (version 1.0.1; Massicotte & South, 2025), rnatualearthdata (version 1.0.0; South et al., 2025) and sf (version 1.0-18; Pebesma & Bivand, 2023). Correlation analysis were performed with
475 stats (version 4.0.2; R Core Team and contributors worldwide, 2020).

This article is dedicated to the memory of our colleague and friend Dr. Gerd Krahmman.

Financial support

This research was supported by the German Federal Ministry for Education and Research (BMBF) via the grant 03G0305A and 03G0305B.

480 References

- Altieri, K. E., Fawcett, S. E., and Hastings, M. G.: Reactive Nitrogen Cycling in the Atmosphere and Ocean, *Annu. Rev. Earth Planet. Sci.*, 49, 523–550, <https://doi.org/10.1146/annurev-earth-083120-052147>, 2021.
- Bange, H. W., Stoltenberg, I., Andersch, T., Arévalo-Martínez, D. L., Atlas, E. L., Babu Suja, A., Barbot, A., Barthelmeß, T., Becker, K. W., Booge, D., Bristow, L. A., Conventz, A., Czeschel, R., Dähnke, K., Deshmukh, S., Duerkop, F., Eisnecker, P.,
485 Engel, A., Engelen, B., Feil, H., Fernández-Juárez, V., Firus, A., Frank, M., Gaye, B., Gledhill, M., Golde, S., Großelindemann, H., Hathorne, E., Henning, S., Hentschel, I., Herrmann, H., Ingeniero, R. C. O., Jacobsen, M., Kiko, R., Lahajnar, N., Lange, K., Löscher, C. R., Marandino, C. A., McKellar, C., Mickenbecker, J., Müller, M., Müller, T., Nazzari, L., Nielsen, L., Ploschke, J., Pohlker, M., Pontiller, B., Poulain, L., Quack, B., Rabe, R., Roa, J., Rolfes, S., Sanders, T., Schlangen, I., Schmidt, L., Schulz, G., Sommer, M., Thamdrup, B., Usinger, J., van Bonn, L., van Pinxteren, M., and Zhong, Q.:
490 Biogeochemistry/atmosphere processes in the Bay of Bengal: A contribution to the 2nd International Indian Ocean Expedition, Cruise No. SO305 10 April - 22 May 2024, Colombo (Sri Lanka) - Singapore (Singapore), Begutachtungspanel Forschungsschiffe, SONNE-Berichte, 86pp, https://doi.org/10.48433/cr_so305, 2024.
- Bristow, L. A., Dalsgaard, T., Tiano, L., Mills, D. B., Bertagnolli, A. D., Wright, J. J., Hallam, S. J., Ulloa, O., Canfield, D. E., Revsbech, N. P., and Thamdrup, B.: Ammonium and nitrite oxidation at nanomolar oxygen concentrations in oxygen
495 minimum zone waters, *Proc. Natl. Acad. Sci.*, 113, 10601–10606, <https://doi.org/10.1073/pnas.1600359113>, 2016.
- Bristow, L. A., Callbeck, C. M., Larsen, M., Altabet, M. A., Dekaezemacker, J., Forth, M., Gauns, M., Glud, R. N., Kuypers, M. M. M., Lavik, G., Milucka, J., Naqvi, S. W. A., Pratihary, A., Revsbech, N. P., Thamdrup, B., Treusch, A. H., and Canfield, D. E.: N₂ production rates limited by nitrite availability in the Bay of Bengal oxygen minimum zone, *Nat. Geosci.*, 10, 24–29, <https://doi.org/10.1038/ngeo2847>, 2017.
- 500 Brunner, B., Contreras, S., Lehmann, M. F., Matantseva, O., Rollog, M., Kalvelage, T., Klockgether, G., Lavik, G., Jetten, M. S. M., Kartal, B., and Kuypers, M. M. M.: Nitrogen isotope effects induced by anammox bacteria, *Proc. Natl. Acad. Sci.*, 110, 18994–18999, <https://doi.org/10.1073/pnas.1310488110>, 2013.
- Buchwald, C. and Casciotti, K. L.: Oxygen isotopic fractionation and exchange during bacterial nitrite oxidation, *Limnol. Oceanogr.*, 55, 1064–1074, <https://doi.org/10.4319/lo.2010.55.3.1064>, 2010.
- 505 Buchwald, C., Santoro, A. E., McIlvin, M. R., and Casciotti, K. L.: Oxygen isotopic composition of nitrate and nitrite produced by nitrifying cocultures and natural marine assemblages, *Limnol. Oceanogr.*, 57, 1361–1375, <https://doi.org/10.4319/lo.2012.57.5.1361>, 2012.
- Casciotti, K. L.: Inverse kinetic isotope fractionation during bacterial nitrite oxidation, *Geochim. Cosmochim. Acta*, 73, 2061–2076, <https://doi.org/10.1016/j.gca.2008.12.022>, 2009.
- 510 Casciotti, K. L.: Nitrogen and Oxygen Isotopic Studies of the Marine Nitrogen Cycle, *Annu. Rev. Mar. Sci.*, 8, 379–407, <https://doi.org/10.1146/annurev-marine-010213-135052>, 2016.

- Casciotti, K. L. and McIlvin, M. R.: Isotopic analyses of nitrate and nitrite from reference mixtures and application to Eastern Tropical North Pacific waters, *Mar. Chem.*, 107, 184–201, <https://doi.org/10.1016/j.marchem.2007.06.021>, 2007.
- 515 Casciotti, K. L., Sigman, D. M., Hastings, M. G., Böhlke, J. K., and Hilkert, A.: Measurement of the Oxygen Isotopic Composition of Nitrate in Seawater and Freshwater Using the Denitrifier Method, *Anal. Chem.*, 74, 4905–4912, <https://doi.org/10.1021/ac020113w>, 2002.
- Casciotti, K. L., Sigman, D. M., and Ward, B. B.: Linking Diversity and Stable Isotope Fractionation in Ammonia-Oxidizing Bacteria, *Geomicrobiol. J.*, 20, 335–353, <https://doi.org/10.1080/01490450303895>, 2003.
- 520 Casciotti, K. L., McIlvin, M., and Buchwald, C.: Oxygen isotopic exchange and fractionation during bacterial ammonia oxidation, *Limnol. Oceanogr.*, 55, 753–762, <https://doi.org/10.4319/lo.2010.55.2.0753>, 2010.
- Dalsgaard, T., Canfield, D. E., Petersen, J., Thamdrup, B., and Acuña-González, J.: N₂ production by the anammox reaction in the anoxic water column of Golfo Dulce, Costa Rica, *Nature*, 422, 606–608, <https://doi.org/10.1038/nature01526>, 2003.
- 525 Dalsgaard, T., Stewart, F. J., Thamdrup, B., De Brabandere, L., Revsbech, N. P., Ulloa, O., Canfield, D. E., and DeLong, E. F.: Oxygen at Nanomolar Levels Reversibly Suppresses Process Rates and Gene Expression in Anammox and Denitrification in the Oxygen Minimum Zone off Northern Chile, *mBio*, 5, 10.1128/mbio.01966-14, <https://doi.org/10.1128/mbio.01966-14>, 2014.
- Deuser, W.: Reducing environments, in: *Chemical Oceanography*, vol. 3, edited by: Riley, J. P. and Skirrow, G., New York, 1–37, 1975.
- 530 DeVries, T., Deutsch, C., Primeau, F., Chang, B., and Devol, A.: Global rates of water-column denitrification derived from nitrogen gas measurements, *Nat. Geosci.*, 5, 547–550, <https://doi.org/10.1038/ngeo1515>, 2012.
- Ditkovsky, S., Resplandy, L., and Busecke, J.: Unique ocean circulation pathways reshape the Indian Ocean oxygen minimum zone with warming, *Biogeosciences*, 20, 4711–4736, <https://doi.org/10.5194/bg-20-4711-2023>, 2023.
- Emery, W. J.: Water Types and Water Masses*, in: *Encyclopedia of Ocean Sciences (Second Edition)*, edited by: Steele, J. H., Academic Press, Oxford, 291–299, <https://doi.org/10.1016/B978-012374473-9.00108-9>, 2001.
- 535 Fawcett, S. E., Ward, B. B., Lomas, M. W., and Sigman, D. M.: Vertical decoupling of nitrate assimilation and nitrification in the Sargasso Sea, *Deep Sea Res. Part Oceanogr. Res. Pap.*, 103, 64–72, <https://doi.org/10.1016/j.dsr.2015.05.004>, 2015.
- Felden, J., Möller, L., Schindler, U., Huber, R., Schumacher, S., Koppe, R., Diepenbroek, M., and Glöckner, F. O.: PANGAEA - Data Publisher for Earth & Environmental Science, *Sci. Data*, 10, 347, <https://doi.org/10.1038/s41597-023-02269-x>, 2023.
- 540 Gaye, B., Nagel, B., Dähnke, K., Rixen, T., and Emeis, K.-C.: Evidence of parallel denitrification and nitrite oxidation in the ODZ of the Arabian Sea from paired stable isotopes of nitrate and nitrite, *Glob. Biogeochem. Cycles*, 27, 1059–1071, <https://doi.org/10.1002/2011GB004115>, 2013.
- Gordon, A. L.: Oceanography of the Indonesian Seas and Their Throughflow, *Oceanography*, 18, 14–27, <https://doi.org/10.5670/oceanog.2005.01>, 2005.
- 545 Granger, J. and Sigman, D. M.: Removal of nitrite with sulfamic acid for nitrate N and O isotope analysis with the denitrifier method, *Rapid Commun. Mass Spectrom.*, 23, 3753–3762, <https://doi.org/10.1002/rcm.4307>, 2009.

- Granger, J. and Wankel, S.: Isotopic overprinting of nitrification on denitrification as a ubiquitous and unifying feature of environmental nitrogen cycling, *Proc. Natl. Acad. Sci.*, 113, E6391–E6400, <https://doi.org/10.1073/pnas.1601383113>, 2016.
- Granger, J., Sigman, D. M., Needoba, J. A., and Harrison, P. J.: Coupled nitrogen and oxygen isotope fractionation of nitrate during assimilation by cultures of marine phytoplankton, *Limnol. Oceanogr.*, 49, 1763–1773, <https://doi.org/10.4319/lo.2004.49.5.1763>, 2004.
- 550
- Granger, J., Sigman, D. M., Lehmann, M. F., and Tortell, P. D.: Nitrogen and oxygen isotope fractionation during dissimilatory nitrate reduction by denitrifying bacteria, *Limnol. Oceanogr.*, 53, 2533–2545, <https://doi.org/10.4319/lo.2008.53.6.2533>, 2008.
- Granger, J., Sigman, D. M., Rohde, M. M., Maldonado, M. T., and Tortell, P. D.: N and O isotope effects during nitrate assimilation by unicellular prokaryotic and eukaryotic plankton cultures, *Geochim. Cosmochim. Acta*, 74, 1030–1040, <https://doi.org/10.1016/j.gca.2009.10.044>, 2010.
- 555
- Gruber, N.: Chapter 1 - The Marine Nitrogen Cycle: Overview and Challenges, in: *Nitrogen in the Marine Environment (Second Edition)*, edited by: Capone, D. G., Bronk, D. A., Mulholland, M. R., and Carpenter, E. J., Academic Press, San Diego, 1–50, <https://doi.org/10.1016/B978-0-12-372522-6.00001-3>, 2008.
- Hansen, H. P.: Determination of oxygen, in: *Methods of Seawater Analysis*, edited by: Grasshoff, K. K. and Ehrhardt, M., John Wiley & Sons, Ltd, 75–89, <https://doi.org/10.1002/9783527613984.ch4>, 1999.
- 560
- Hansen, H. P. and Koroleff, F.: Determination of nutrients, in: *Methods of Seawater Analysis*, John Wiley & Sons, Ltd, 159–228, <https://doi.org/10.1002/9783527613984.ch10>, 1999.
- Harms, N. C., Lahajnar, N., Gaye, B., Rixen, T., Dähnke, K., Ankele, M., Schwarz-Schampera, U., and Emeis, K.-C.: Nutrient distribution and nitrogen and oxygen isotopic composition of nitrate in water masses of the subtropical southern Indian Ocean, *Biogeosciences*, 16, 2715–2732, <https://doi.org/10.5194/bg-16-2715-2019>, 2019.
- 565
- Holmes, R. M., Aminot, A., K erouel, R., Hooker, B. A., and Peterson, B. J.: A simple and precise method for measuring ammonium in marine and freshwater ecosystems, *Can. J. Fish. Aquat. Sci.*, 56, 1801–1808, <https://doi.org/10.1139/f99-128>, 1999.
- Howell, E. A., Doney, S. C., Fine, R. A., and Olson, D. B.: Geochemical estimates of denitrification in the Arabian Sea and the Bay of Bengal during WOCE, *Geophys. Res. Lett.*, 24, 2549–2552, <https://doi.org/10.1029/97GL01538>, 1997.
- 570
- Jain, V., Shankar, D., Vinayachandran, P. N., Kankonkar, A., Chatterjee, A., Amol, P., Almeida, A. M., Michael, G. S., Mukherjee, A., Chatterjee, M., Fernandes, R., Luis, R., Kamble, A., Hegde, A. K., Chatterjee, S., Das, U., and Neema, C. P.: Evidence for the existence of Persian Gulf Water and Red Sea Water in the Bay of Bengal, *Clim. Dyn.*, 48, 3207–3226, <https://doi.org/10.1007/s00382-016-3259-4>, 2017.
- 575
- Johnson, K. S., Riser, S. C., and Ravichandran, M.: Oxygen Variability Controls Denitrification in the Bay of Bengal Oxygen Minimum Zone, *Geophys. Res. Lett.*, 46, 804–811, <https://doi.org/10.1029/2018GL079881>, 2019.
- Junior, O. de O. C.: Water Masses at the Surface of the Indian Ocean, *Eur. J. Environ. Earth Sci.*, 4, 11–21, <https://doi.org/10.24018/ejgeo.2023.4.2.389>, 2023.
- 580
- Kalvelage, T., Jensen, M. M., Contreras, S., Revsbech, N. P., Lam, P., G nter, M., LaRoche, J., Lavik, G., and Kuypers, M. M.: Oxygen sensitivity of anammox and coupled N-cycle processes in oxygen minimum zones, *PloS One*, 6, e29299, <https://doi.org/10.1371/journal.pone.0029299>, 2011.

- Karsh, K. L., Granger, J., Kritee, K., and Sigman, D. M.: Eukaryotic Assimilatory Nitrate Reductase Fractionates N and O Isotopes with a Ratio near Unity, *Environ. Sci. Technol.*, 46, 5727–5735, <https://doi.org/10.1021/es204593q>, 2012.
- Kassambara, A.: ggpubr: “ggplot2” Based Publication Ready Plots, 2023.
- 585 Kawano, T.: Method for Salinity (Conductivity Ratio) Measurement, GO-SHIP Repeat Hydrogr. Man. Collect. Expert Rep. Guidel. Eds Al, IOCCP Report, <https://doi.org/10.25607/OBP-1339>, 2010.
- Kendall, C., Elliott, E. M., and Wankel, S. D.: Tracing Anthropogenic Inputs of Nitrogen to Ecosystems, in: *Stable Isotopes in Ecology and Environmental Science*, John Wiley & Sons, Ltd, 375–449, <https://doi.org/10.1002/9780470691854.ch12>, 2007.
- 590 Kim, Y., Rho, T., and Kang, D.-J.: Oxygen isotope composition of seawater and salinity in the western Indian Ocean: Implications for water mass mixing, *Mar. Chem.*, 237, 104035, <https://doi.org/10.1016/j.marchem.2021.104035>, 2021.
- Knapp, A. N., DiFiore, P. J., Deutsch, C., Sigman, D. M., and Lipschultz, F.: Nitrate isotopic composition between Bermuda and Puerto Rico: Implications for N₂ fixation in the Atlantic Ocean, *Glob. Biogeochem. Cycles*, 22, GB3014, <https://doi.org/10.1029/2007GB003107>, 2008.
- 595 Knowles, R.: Denitrification, *Microbiol. Rev.*, 46, 43–70, <https://doi.org/10.1128/mr.46.1.43-70.1982>, 1982.
- Kobayashi, K., Makabe, A., Yano, M., Oshiki, M., Kindaichi, T., Casciotti, K. L., and Okabe, S.: Dual nitrogen and oxygen isotope fractionation during anaerobic ammonium oxidation by anammox bacteria, *ISME J.*, 13, 2426–2436, <https://doi.org/10.1038/s41396-019-0440-x>, 2019.
- Kool, D. M., Wrage, N., Oenema, O., Dolfing, J., and Van Groenigen, J. W.: Oxygen exchange between (de)nitrification intermediates and H₂O and its implications for source determination of NO₃⁻ and N₂O: a review, *Rapid Commun. Mass Spectrom. RCM*, 21, 3569–3578, <https://doi.org/10.1002/rcm.3249>, 2007.
- 600 Kumar, S., Ramesh, R., Sardesai, S., and Sheshshayee, M. S.: High new production in the Bay of Bengal: Possible causes and implications, *Geophys. Res. Lett.*, 31, L18304, <https://doi.org/10.1029/2004GL021005>, 2004.
- LeGrande, A. N. and Schmidt, G. A.: Global gridded data set of the oxygen isotopic composition in seawater, *Geophys. Res. Lett.*, 33, <https://doi.org/10.1029/2006GL026011>, 2006.
- 605 Löscher, C. R., Mohr, W., Bange, H. W., and Canfield, D. E.: No nitrogen fixation in the Bay of Bengal?, *Biogeosciences*, 17, 851–864, <https://doi.org/10.5194/bg-17-851-2020>, 2020.
- Marshall, T. A., Sigman, D. M., Beal, L. M., Foreman, A., Martínez-García, A., Blain, S., Campbell, E., Fripiat, F., Granger, R., Harris, E., Haug, G. H., Marconi, D., Oleynik, S., Rafter, P. A., Roman, R., Sinyanya, K., Smart, S. M., and Fawcett, S. E.: The Agulhas Current Transports Signals of Local and Remote Indian Ocean Nitrogen Cycling, *J. Geophys. Res. Oceans*, 128, e2022JC019413, <https://doi.org/10.1029/2022JC019413>, 2023.
- 610 Martin, T. S. and Casciotti, K. L.: Paired N and O isotopic analysis of nitrate and nitrite in the Arabian Sea oxygen deficient zone, *Deep Sea Res. Part Oceanogr. Res. Pap.*, 121, 121–131, <https://doi.org/10.1016/j.dsr.2017.01.002>, 2017.
- Massicotte, P. and South, A.: *rnaturalearth: World Map Data from Natural Earth*, 2025.
- 615 Naqvi, S. W. A., DeSousa, S. N., and Reddy, C. V. G.: Relationship between nutrients and dissolved oxygen with special reference to water masses in westrn Bay of Bengal, *Indian J. Geo-Mar. Sci.*, 7, 15–17, 1978.

- Naqvi, S. W. A., Yoshinari, T., Brandes, J. A., Devol, A. H., Jayakumar, D. A., Narvekar, P. V., Altabet, M. A., and Codispoti, L. A.: Nitrogen isotopic studies in the suboxic Arabian Sea, *Proc. Indian Acad. Sci. - Earth Planet. Sci.*, 107, 367–378, <https://doi.org/10.1007/BF02841603>, 1998.
- 620 Okabe, S., Ye, S., Lan, X., Nukada, K., Zhang, H., Kobayashi, K., and Oshiki, M.: Oxygen tolerance and detoxification mechanisms of highly enriched planktonic anaerobic ammonium-oxidizing (anammox) bacteria, *ISME Commun.*, 3, 45, <https://doi.org/10.1038/s43705-023-00251-7>, 2023.
- Pebesma, E. and Bivand, R.: *Spatial Data Science: With Applications in R*, Chapman and Hall/CRC, New York, 314 pp., <https://doi.org/10.1201/9780429459016>, 2023.
- 625 Peng, X., Fawcett, S. E., van Oostende, N., Wolf, M. J., Marconi, D., Sigman, D. M., and Ward, B. B.: Nitrogen uptake and nitrification in the subarctic North Atlantic Ocean, *Limnol. Oceanogr.*, 63, 1462–1487, <https://doi.org/10.1002/lno.10784>, 2018.
- Phillips, H. E., Menezes, V. V., Nagura, M., McPhaden, M. J., Vinayachandran, P. N., and Beal, L. M.: Indian Ocean circulation[Ⓢ], in: *The Indian Ocean and its Role in the Global Climate System*, edited by: Ummerhofer, C. C. and Hood, R. R., Elsevier, 169–203, <https://doi.org/10.1016/B978-0-12-822698-8.00012-3>, 2024.
- 630 The R Stats Package, Version 4.0.2: <https://www.rdocumentation.org/packages/stats/versions/3.6.2/topics/prcomp>, last access: 29 January 2021.
- Rahman, A., Khan, M. A., Singh, A., and Kumar, S.: Hydrological characteristics of the Bay of Bengal water column using $\delta^{18}\text{O}$ during the Indian summer monsoon, *Cont. Shelf Res.*, 226, 104491, <https://doi.org/10.1016/j.csr.2021.104491>, 2021.
- 635 Rao, C. K., Naqvi, S. W. A., Kumar, M. D., Varaprasad, S. J. D., Jayakumar, D. A., George, M. D., and Singbal, S. Y. S.: Hydrochemistry of the Bay of Bengal: possible reasons for a different water-column cycling of carbon and nitrogen from the Arabian Sea, *Mar. Chem.*, 47, 279–290, [https://doi.org/10.1016/0304-4203\(94\)90026-4](https://doi.org/10.1016/0304-4203(94)90026-4), 1994.
- Rixen, T., Cowie, G., Gaye, B., Goes, J., do Rosário Gomes, H., Hood, R. R., Lachkar, Z., Schmidt, H., Segsneider, J., and Singh, A.: Reviews and syntheses: Present, past, and future of the oxygen minimum zone in the northern Indian Ocean, *Biogeosciences*, 17, 6051–6080, <https://doi.org/10.5194/bg-17-6051-2020>, 2020.
- 640 Sardessai, S., Ramaiah, N., Kumar, S., and Sousa, S. de: Influence of environmental forcings on the seasonality of dissolved oxygen and nutrients in the Bay of Bengal, *J. Mar. Res.*, 65, 301–316, 2007.
- Sarma, V. V. S. S.: An evaluation of physical and biogeochemical processes regulating the oxygen minimum zone in the water column of the Bay of Bengal, *Glob. Biogeochem. Cycles*, 16, 46-1-46–10, <https://doi.org/10.1029/2002GB001920>, 2002.
- 645 Sarma, V. V. S. S.: Biogeochemistry of carbon, nitrogen and oxygen in the Bay of Bengal: New insights through re-analysis of data, *J. Earth Syst. Sci.*, 131, 159, <https://doi.org/10.1007/s12040-022-01915-z>, 2022.
- Sarma, V. V. S. S. and Udaya Bhaskar, T. V. S.: Ventilation of Oxygen to Oxygen Minimum Zone Due to Anticyclonic Eddies in the Bay of Bengal, *J. Geophys. Res. Biogeosciences*, 123, 2145–2153, <https://doi.org/10.1029/2018JG004447>, 2018.
- Sarma, V. V. S. S., Krishna, M. S., Viswanadham, R., Rao, G. D., Rao, V. D., Sridevi, B., Kumar, B. S. K., Prasad, V. R., Subbaiah, C. V., Acharyya, T., and Bandopadhyay, D.: Intensified oxygen minimum zone on the western shelf of Bay of Bengal during summer monsoon: influence of river discharge, *J. Oceanogr.*, 69, 45–55, <https://doi.org/10.1007/s10872-012-0156-2>, 2013.
- 650

- 655 Sarma, V. V. S. S., Rao, G. D., Viswanadham, R., Sherin, C. K., Salisbury, J., Omand, M. M., Mahadevan, A., Murty, V. S. N., Shroyer, E. L., Baumgartner, M., and Stafford, K. M.: Effects of Freshwater Stratification on Nutrients, Dissolved Oxygen, and Phytoplankton in the Bay of Bengal, *Oceanography*, 29, 222–231, 2016.
- Saxena, H., Sahoo, D., Khan, M. A., Kumar, S., Sudheer, A. K., and Singh, A.: Dinitrogen fixation rates in the Bay of Bengal during summer monsoon, *Environ. Res. Commun.*, 2, 051007, <https://doi.org/10.1088/2515-7620/ab89fa>, 2020.
- Schott, F. A. and McCreary, J. P.: The monsoon circulation of the Indian Ocean, *Prog. Oceanogr.*, 51, 1–123, [https://doi.org/10.1016/S0079-6611\(01\)00083-0](https://doi.org/10.1016/S0079-6611(01)00083-0), 2001.
- 660 Schott, F. A., Xie, S.-P., and McCreary Jr., J. P.: Indian Ocean circulation and climate variability, *Rev. Geophys.*, 47, RG1002, <https://doi.org/10.1029/2007RG000245>, 2009.
- Sen Gupta, R., De Sousa, S. N., and Joseph, T.: On nitrogen and phosphorus in the western Bay of Bengal, *Indian J. Geo-Mar. Sci.*, 6, 107–110, 1977.
- 665 Sengupta, S., Parekh, A., Chakraborty, S., Ravi Kumar, K., and Bose, T.: Vertical variation of oxygen isotope in Bay of Bengal and its relationships with water masses, *J. Geophys. Res. Oceans*, 118, 6411–6424, <https://doi.org/10.1002/2013JC008973>, 2013.
- Shee, A., Sil, S., and Gangopadhyay, A.: Recent changes in the upper oceanic water masses over the Indian Ocean using Argo data, *Sci. Rep.*, 13, 20252, <https://doi.org/10.1038/s41598-023-47658-9>, 2023.
- 670 Sheehan, P. M. F., Webber, B. G. M., Sanchez-Franks, A., Matthews, A. J., Heywood, K. J., and Vinayachandran, P. N.: Injection of Oxygenated Persian Gulf Water Into the Southern Bay of Bengal, *Geophys. Res. Lett.*, 47, e2020GL087773, <https://doi.org/10.1029/2020GL087773>, 2020.
- Shetye, S. R.: The movement and implications of the Ganges–Brahmaputra runoff on entering the Bay of Bengal, *Curr. Sci.*, 64, 32–38, 1993.
- 675 Shiozaki, T., Ijichi, M., Kodama, T., Takeda, S., and Furuya, K.: Heterotrophic bacteria as major nitrogen fixers in the euphotic zone of the Indian Ocean, *Glob. Biogeochem. Cycles*, 28, 1096–1110, <https://doi.org/10.1002/2014GB004886>, 2014.
- Sigman, D. M. and Fripiat, F.: Nitrogen Isotopes in the Ocean, *Encycl. Ocean Sci. Third Ed.*, 1, 263–278, <https://doi.org/10.1016/B978-0-12-409548-9.11605-7>, 2019.
- 680 Sigman, D. M., Altabet, M. A., McCorkle, D. C., Francois, R., and Fischer, G.: The $\delta^{15}\text{N}$ of nitrate in the Southern Ocean: Nitrogen cycling and circulation in the ocean interior, *J. Geophys. Res. Oceans*, 105, 19599–19614, <https://doi.org/10.1029/2000JC000265>, 2000.
- Sigman, D. M., Casciotti, K. L., Andreani, M., Barford, C., Galanter, M., and Böhlke, J. K.: A Bacterial Method for the Nitrogen Isotopic Analysis of Nitrate in Seawater and Freshwater, *Anal. Chem.*, 73, 4145–4153, <https://doi.org/10.1021/ac010088e>, 2001.
- 685 Sigman, D. M., Granger, J., DiFiore, P. J., Lehmann, M. M., Ho, R., Cane, G., and van Geen, A.: Coupled nitrogen and oxygen isotope measurements of nitrate along the eastern North Pacific margin, *Glob. Biogeochem. Cycles*, 19, <https://doi.org/10.1029/2005GB002458>, 2005.

- Sigman, D. M., DiFiore, P. J., Hain, M. P., Deutsch, C., Wang, Y., Karl, D. M., Knapp, A. N., Lehmann, M. F., and Pantoja, S.: The dual isotopes of deep nitrate as a constraint on the cycle and budget of oceanic fixed nitrogen, *Deep Sea Res. Part Oceanogr. Res. Pap.*, 56, 1419–1439, <https://doi.org/10.1016/j.dsr.2009.04.007>, 2009.
- 690 Snider, D. M., Spoelstra, J., Schiff, S. L., and Venkiteswaran, J. J.: Stable Oxygen Isotope Ratios of Nitrate Produced from Nitrification: ^{18}O -Labeled Water Incubations of Agricultural and Temperate Forest Soils, *Environ. Sci. Technol.*, 44, 5358–5364, <https://doi.org/10.1021/es1002567>, 2010.
- South, A., Michael, S., and Massicotte, P.: *rnaturalearthdata*: World Vector Map Data from Natural Earth Used in “*rnaturalearth*,” 2025.
- 695 Sprintall, J. and Tomczak, M.: On the formation of central water and thermocline ventilation in the southern hemisphere, *Deep Sea Res. Part Oceanogr. Res. Pap.*, 40, 827–848, [https://doi.org/10.1016/0967-0637\(93\)90074-D](https://doi.org/10.1016/0967-0637(93)90074-D), 1993.
- Sprintall, J., Wijffels, S. E., Molcard, R., and Jaya, I.: Direct estimates of the Indonesian Throughflow entering the Indian Ocean: 2004–2006, *J. Geophys. Res. Oceans*, 114, C07001, <https://doi.org/10.1029/2008JC005257>, 2009.
- 700 Sridevi, B. and Sarma, V. V. S. S.: A revisit to the regulation of oxygen minimum zone in the Bay of Bengal, *J. Earth Syst. Sci.*, 129, 107, <https://doi.org/10.1007/s12040-020-1376-2>, 2020.
- Srivastava, R., Ramesh, R., Prakash, S., Anilkumar, N., and Sudhakar, M.: Oxygen isotope and salinity variations in the Indian sector of the Southern Ocean, *Geophys. Res. Lett.*, 34, <https://doi.org/10.1029/2007GL031790>, 2007.
- 705 Strous, M., Fuerst, J. A., Kramer, E. H. M., Logemann, S., Muyzer, G., van de Pas-Schoonen, K. T., Webb, R., Kuenen, J. G., and Jetten, M. S. M.: Missing lithotroph identified as new planctomycete, *Nature*, 400, 446–449, <https://doi.org/10.1038/22749>, 1999.
- Sun, X., Frey, C., Garcia-Robledo, E., Jayakumar, A., and Ward, B. B.: Microbial niche differentiation explains nitrite oxidation in marine oxygen minimum zones, *ISME J.*, 15, 1317–1329, <https://doi.org/10.1038/s41396-020-00852-3>, 2021.
- Sun, X., Frey, C., and Ward, B. B.: Nitrite Oxidation Across the Full Oxygen Spectrum in the Ocean, *Glob. Biogeochem. Cycles*, 37, e2022GB007548, <https://doi.org/10.1029/2022GB007548>, 2023.
- 710 Sverdrup, H. U., Johnson, M. W., and Fleming, R. H.: *The Oceans Their Physics, Chemistry, and General Biology*, Prentice-Hall, New York, 1060 pp., 1942.
- Tiedje, J. M.: Ecology of denitrification and dissimilatory nitrate reduction to ammonium, in: *Biology of anaerobic microorganisms*, edited by: Zehnder, A. J. B., John Wiley and Sons, New York, 179–244, 1988.
- 715 Tomczak, M. and Godfrey, J. S.: CHAPTER 11 - The Indian Ocean, in: *Regional Oceanography*, edited by: Tomczak, M. and Godfrey, J. S., Pergamon, Amsterdam, 193–220, <https://doi.org/10.1016/B978-0-08-041021-0.50015-1>, 1994.
- Trimmer, M., Nicholls, J. C., and Deflandre, B.: Anaerobic Ammonium Oxidation Measured in Sediments along the Thames Estuary, United Kingdom, *Appl. Environ. Microbiol.*, 69, 6447–6454, <https://doi.org/10.1128/AEM.69.11.6447-6454.2003>, 2003.
- 720 Ummenhofer, C. C. and Hood, R. R. (Eds.): *The Indian Ocean and its Role in the Global Climate System*, 1st ed., Elsevier, 2024.

- Vinayachandran, P. N., Masumoto, Y., Mikawa, T., and Yamagata, T.: Intrusion of the Southwest Monsoon Current into the Bay of Bengal, *J. Geophys. Res. Oceans*, 104, 11077–11085, <https://doi.org/10.1029/1999JC900035>, 1999.
- Wankel, S. D., Kendall, C., Pennington, J. T., Chavez, F. P., and Paytan, A.: Nitrification in the euphotic zone as evidenced by nitrate dual isotopic composition: Observations from Monterey Bay, California, *Glob. Biogeochem. Cycles*, 21, <https://doi.org/10.1029/2006GB002723>, 2007.
- 725
- Ward, B. B.: How Nitrogen Is Lost, *Science*, 341, 352–353, <https://doi.org/10.1126/science.1240314>, 2013.
- Wickham, H., Chang, W., Henry, L., Pedersen, T. L., Takahashi, K., Wilke, C., Woo, K., Yutani, H., Dunnington, D., and van den Brand, T.: *ggplot2: Elegant Graphics for Data Analysis*, Springer-Verlag, New York, 2016.
- Winkler, L. W.: Die Bestimmung des im Wasser gelösten Sauerstoffes, *Berichte Dtsch. Chem. Ges.*, 21, 2843–2854, <https://doi.org/10.1002/cber.188802102122>, 1888.
- 730
- Wyrtki, K.: *Oceanographic atlas of the International Indian Ocean Expedition*, National Science Foundation, Washington, DC, 531 pp., 1971.
- Wyrtki, K.: An equatorial jet in the Indian ocean, *Science*, 181, 262–264, <https://doi.org/10.1126/science.181.4096.262>, 1973.
- You, Y.: Seasonal variations of thermocline circulation and ventilation in the Indian Ocean, *J. Geophys. Res. Oceans*, 102, 10391–10422, <https://doi.org/10.1029/96JC03600>, 1997.
- 735
- You, Y. and Tomczak, M.: Thermocline circulation and ventilation in the Indian Ocean derived from water mass analysis, *Deep Sea Res. Part Oceanogr. Res. Pap.*, 40, 13–56, [https://doi.org/10.1016/0967-0637\(93\)90052-5](https://doi.org/10.1016/0967-0637(93)90052-5), 1993.